PARASITIC NOISE FROM PROBES AND STRUTS IN FLOWS

by

Leif Erik Hoglund

B.ApSc, University of British Columbia

A THESIS SUBMITTED IN PARTIAL FULFILMENT OF

THE REQUIREMENTS FOR THE DEGREE OF

MASTER OF APPLIED SCIENCE

in the Department

of

Mechanical Engineering

We accept this thesis as conforming to the

required standard

THE UNIVERSITY OF BRITISH COLUMBIA

October, 1975

In presenting this thesis in partial fulfilment of the requirements for an advanced degree at the University of British Columbia, I agree that the Library shall make it freely available for reference and study. I further agree that permission for extensive copying of this thesis for scholarly purposes may be granted by the Head of my Department or by his representatives. It is understood that copying or publication of this thesis for financial gain shall not be allowed without my written permission.

Department of MECHANICAL ENG.

The University of British Columbia
2075 Wesbrook Place
Vancouver, Canada
V6T 1W5

Date OCT 7/ 75

SUMMARY

When a fast-responding static pressure probe is inserted into a flow, there are several possible mechanisms for the generation of extraneous noise. If the probe signal is cross-correlated with the far field sound, then the "probe noise" may contribute a dominant fraction of the total correlatable noise in the source region. For a standard probe, there is likely to be contamination from the tip due to large fluctuating side forces, and from the stem, due to drag fluctuations. A theoretical model is suggested for predicting the distortion of "causality" correlation signatures (obtained when in-flow probes are cross-correlated with the far field sound), due to the probe tip contamination. The predicted shapes agree well with experiment.

In the experimental investigations, the contaminated portion of the causality correlation signature is displaced in time from the "true" jet pressure correlation. The unexpected result is the absence of any significant jet pressure correlation. This leads to the conclusion that the extent of jet noise sources may be very small, so that probing devices inserted into the flow will generally produce a large portion of the total correlation.

TABLE OF CONTENTS

LIST OF FIGURES

Figure

Figure

NOTATION

$p^{(o)'}$	fluctuating static pressure measured by the in-flow probing device
$p^{(o)}$	fluctuating static jet pressure
p_n	surface pressure on the probe
p	far field pressure
$\underline{x}$	space coordinate, used to indicate the distance from a turbulent source to the far field microphone
$\underline{x}'$	space coordinate, indicates distance from a point on the probe to the far field microphone
$\underline{y}$	space cordinate, indicates a point position in the turbulence measured from the pressure taps
y'	indicates a point on the probe surface measured from the pressure taps
$\underline{r}$	space coordinate, indicates the distance from the pressure taps to the far field microphone
x_o	distance from the jet exit plane in the streamwise direction
y_o	radial distance from the jet centreline
d	probe diameter
D	jet diameter
u,v,w	fluctuating velocity components (primed values denote root-mean-square)
U_c	convection velocity
V_j	velocity at the jet exit plane
M_j	Mach number at the jet exit plane (V_j/c_o)
c_o	speed of sound
ρ	density
θ	angle between a normal to the probe surface and the far field microphone

β	angle between a side force component on the probe surface and and the far field microphone located in the same plane
γ	angle between a surface normal on the probe and the plane containing both the far field microphone and the probe
u_n	normal surface velocity
t	time
t'	some time other than t
τ	a time difference given by t-t'
$\hat{t}$	retarded time = $t - \frac{x}{c}$
$\hat{\tau}$	$\tau - \frac{x}{c}$
L	integral length scale
T	integral time scale in convecting frame of reference
Y_t	distance from pressure taps to probe tip
Y_{peak}	distance from the pressure taps to the point on the probe tip where an incidence-induced side force distribution has maximum value
V_c	correlation volume
T_{ij}	Lighthill's stress tensor
S	surface
ξ	space separation vector
V	volume
$C_m(\tau)$	correlation coefficient -- $\overline{P P^{(o)'}}(\tau) / ((\rho_j V_j^2)^2 M_j^2 D/2)$
$C(\tau)$	correlation coefficient -- $\overline{P P^{(o)'}}(\tau) / (\sqrt{\overline{P^{(o)2}}} \sqrt{\overline{P^2}})$

ACKNOWLEDGEMENTS

Sincere thanks must go to Dr. T.E. Siddon. Only his patient guidance and his invaluable expertise made this work possible.

Thanks also go to Dr. Huw Davies for his interest and helpful suggestions, and to Brian Davis for acquiring some of the data.

A special thank-you goes to my wife, Susan, for her considerable patience while typing this thesis.

This research was funded under National Research Council of Canada Grant A-7106, and Defense Research Board Grant 9611-03.

1. INTRODUCTION

1.1 Purpose and Scope

Since the advent of jet propulsion there have been substantial reductions in the noise from jets. The most significant improvement has been through the development of high by-pass ratio engines which effectively reduce the average jet exit velocity. Other reductions result from new turbine designs and acoustically treated flow passages (i.e., duct linings). Further reductions will only be possible however, if more is known about the location of sources within jet exhausts. If the individual contributions from each unit of volume in the source region can be determined, then the localized effects of various suppression techniques and nozzle configurations can be determined more accurately.

A source location technique which has shown considerable promise is the so-called "causality" correlation technique. In this technique, the strength of noise sources is determined by the degree of correlation between a signal in the supposed source region (the cause) and the resulting noise detected in the far field. The simplest source signal to measure is the fluctuating static pressure in the jet. Unfortunately, certain errors will result in the correlation signature when this is done. The most serious error is due to the generation of extraneous noise by the probing device in the flow. This "probe noise" is sensed by the far field microphone and will contaminate the correlation signature.

The purpose in this work has been to examine the processes which lead to contamination of the correlation signature. Empirical methods are suggested for estimating the extraneous noise fractions, which should lead to ideas for minimizing the contamination effect. Experimental results are presented and compared to an empirical model. Good agreement is indicated.

1.2 Motivation

It can be shown[17] that if a jet is made up of N uncorrelated sources then the relative contribution to the total far field sound $\overline{p^2}$ from a single coherent volume source will be given by a normalized correlation coefficient:

$$\overline{p^{(o)'}P(\tau)}\Big/\left(\sqrt{\overline{p^{(o)'2}}}\sqrt{\overline{P^2}}\right) = C_{MAX}(\tau) \qquad (1.1)$$

where $p^{(o)'}$ = measured jet pressure fluctuation. Furthermore, if the sources are of relatively equal strength, the number of sources can be estimated as: $\frac{1}{C^2_{MAX}} \doteq N$

Although several researchers have begun using the causality technique for measuring source strength in recent years, the agreement amongst different experimenters has not been good. The table below lists the results for normalized cross-correlation coefficients for several different experimental set-ups.

	PROBE TYPE & SIZE	PROBE POSITION	JET DIAMETER (INCHES)	MACH NUMBER	d/D	COEFFICIENT C_{max}
Meecham[8] & Hurdle	B&K ¼" with standard nose cone	$\frac{x_o}{D}$ =5.2 $\frac{y_o}{D}$ =1 θ=90°	6.5	.52-.99	.0385	.006-.011
Rackl[12]	special foil type d≃1/8"	$\frac{x_o}{D}$ =3 $\frac{y_o}{D}$ =½ θ=90°	1.5	.3	≃.083	.08
Lee & Ribner[6]	hot wire	$\frac{x_o}{D}$ =5 to 6 $\frac{y_o}{D}$ =½ θ=40°	.75	.3	∿0	.02
Scharton[14] & White	1/8" B&K with nose cone	$\frac{x_o}{D}$ =6.4 $\frac{y_o}{D}$ =0 θ=30°	.625	.99	.20	.5

θ = angle measured between the jet axis and the far field microphone

x_o = distance from jet exit plane

y_o = radial distance from the jet centre line

d = probe diameter

D = jet diameter

Note that the value of C_{max} is quite variable and generally increases as the probe size becomes a larger and larger fraction of the jet diameter. Ideally we would expect C_{max} to have a relatively invarient value, independent of the measurement. There are three possible causes for the differences in the previous table:

1. differing experimental conditions
2. errors in measuring the fluctuating static pressure
3. probe noise

The first cause, due to differing experimental conditions, is certainly an important factor in explaining the differences. Scharton and White, for example, filtered the jet pressure signal around the jet Strouhal frequency (peak noise frequency). If the pressure spectrum at a point in the flow does not peak at the same frequency as the overall jet spectrum, such filtering will lead to an underestimate of $\overline{p^{(o)2}}$. According to equation (1.1) this will tend to overestimate the causality correlation coefficient. Scharton and White's experiments were also taken on-axis, while the others were offset radially to the position of maximum shear. Since the root-mean-square jet pressures are lower on the jet axis, this will again tend to overestimate the correlation coefficient. The wide range of Mach numbers over which the different experiments were conducted could also tend to introduce variation, since the jet coherence may indeed be expected to increase with Mach number.

The problem of the measurement of static pressure in a turbulent flow is well known, and will also introduce error. Siddon[15] has shown however, that if the flow can be considered locally quasi-steady, and if the measuring probe is properly aligned with the average flow, then the error in the measurement of fluctuation pressure will be $\simeq B\rho(v^2+w^2-\overline{v^2}-\overline{w^2})$ where $B\simeq-\frac{1}{4}$ to $-\frac{1}{2}$, and v and w are the fluctuating cross-flow velocity components normal to the probe axis. If the pressure in the jet varies roughly as $\rho u\overline{U}$ then the maximum expected error will be about 20%. Recent work by Planchon[10] supports this.

It is a premise of this paper that it is the third possible cause, probe noise, that contributes much of the variation in the results on the previous page. The work by Meecham and Hurdle on a large sized jet is done with a rather small probing device relative to the jet diameter and results in a small normalized coefficient. The hot wire measurements by Lee and Ribner also result in a small correlation coefficient, whereas the results by Scharton & White and Rackl are much higher using larger probing devices.

If much of the variation is indeed due to the probe size and configuration used, then it should be possible to show this in a systematic way by varying probe size or geometry.

1.3 Work Done by Others

Rackl[12] found that if a probe of the type shown in Figure 1 was shortened or lengthened, the correlation signature would change. Siddon[17] at that time proposed a ratio for predicting extraneous noise due to the probe which he called the "probe contamination ratio". If a probe such as that shown in Figure 2 is imbedded in a turbulent flow, the tip will experience certain lift and side forces and the stem will undergo fluctuating drag forces. As these forces fluctuate with time, they will appear as acoustic dipole sources, hence radiating sound. The "probe contamination ratio" was meant as a crude estimate of the ratio of unwanted noise due to lift, side or drag forces acting on the probe, to the noise coming from an adjacent correlated volume element of turbulence. For contamination due to drag, he found that the probe contamination ratio

$$PCR_{drag} \simeq K_D \left(\frac{d}{D}\right)^2 \frac{1}{M_{loc}^2}$$

where d=probe diameter
D=jet diameter
M_{loc} = local Mach number

For lift or side forces,

$$PCR_{lift} \simeq K_L \left(\frac{d}{D}\right)^4 \frac{1}{M_{loc}^2}$$

As expected, smaller probes will have a lower PCR than larger probes, and the contamination should reduce with increasing Mach number. Siddon estimated that K_D has a nominal value of about 40, and K_L about 80. However these values are only crude estimates (for $x_o/D=4.0$, $y_o/D=\frac{1}{2}$). The actual values must certainly depend on the position of the probe within the jet flow, and on the detailed probe geometry.

Although Siddon has been able to estimate the relative proportion of probe noise to jet noise, and thereby estimate the degree of possible contamination, the results have not been verified experimentally. Also, if the form of the contaminated cross-correlation function can be predicted and it agrees with experimental fact, then this will lead to more rigorous ideas about the physical parameters and properties of the flow field which govern the contamination of the correlation functions.

2. AEROACOUSTIC THEORY

2.1 Background

From the statements of mass and momentum conservation, it is possible to form a non-homogeneous wave equation.

mass: $$\frac{\partial \rho}{\partial t} + \frac{\partial (\rho u_i)}{\partial x_i} = 0$$

momentum: $$\rho \frac{\partial u_i}{\partial t} + \rho u_j \frac{\partial u_i}{\partial x_j} + \frac{\partial p}{\partial x_i} - \frac{\partial \tau_{ij}}{\partial x_j} = 0$$

Combining gives:

$$\frac{\partial^2 \rho}{\partial t^2} - c_o^2 \nabla^2 \rho = \frac{\partial^2 T_{ij}}{\partial x_i \partial x_j} \tag{2.1}$$

where $T_{ij} = \rho u_i u_j + p\delta_{ij} - \tau_{ij} - c^2 \rho \delta_{ij}$

c_o = ambient speed of sound

p, ρ = pressure, density - including both mean and fluctuating parts

The dependent variables can be written as the sum of a constant part and a fluctuating part at each point in space, so that equation (2.1) can be rewritten for the fluctuating components as:

$$\frac{\partial^2 \rho'}{\partial t^2} - c_o^2 \nabla^2 \rho' = \frac{\partial^2 T_{ij}'}{\partial x_i \partial x_j} \tag{2.2}$$

(Lighthill's equation)

For acoustic processes which can be considered adiabatic (as in shock-free flows) the isentropic equation of state can be assumed:

$$p' = \left(\frac{\partial p}{\partial \rho}\right)_s \rho' = c_o^2 \rho'$$

This allows equation (2.2) to be written in terms of the fluctuating pressure.

$$(2.3) \qquad \frac{1}{c_o^2}\frac{\partial^2 p'}{\partial t^2} - \nabla^2 p' = \frac{\partial^2 T_{ij}}{\partial x_i \partial x_j}$$

In turbulent flows it is usual to assume that viscous stresses are small compared to Reynold's stresses ($\tau_{ij} << \rho u_i u_j$), thus equation (2.3) can be further simplified.

$$(2.4) \qquad \frac{1}{c_o^2}\frac{\partial^2 p'}{\partial t^2} - \nabla^2 p' = \frac{\partial^2 \rho u_i u_j}{\partial x_i \partial x_j}$$

There are two well-known solutions to equation (2.4). The first, due to Proudman[11], is given below:

$$(2.5) \qquad p(\underline{x},t) \doteq \frac{1}{4\pi c_o^2 \underline{x}} \int_V \left[\frac{\partial^2}{\partial t^2}(\rho u_x^2)\right]_{\hat{t}} dV(\underline{y})$$

$p(\underline{x},t)$ is the acoustic pressure received in the far field due to, in this case, momentum fluctuations of the turbulence in the direction of the observer (see Figure 3). These momentum fluctuations can be thought of as noise emitters. The second time derivative of these fluctuations must be integrated over the source region to give the contribution to the far field pressure from that region. The square brackets denote evaluation at the retarded time $\hat{t}=t-\underline{x}/c_o$ where $\underline{x}$ is the distance from the source to the observer, and c_o is the speed of sound.

An equivalent solution to equation (2.4) has been suggested by Ribner.[13]

$$(2.6)\quad P(\underline{x},t) = \frac{-1}{4\pi c_o^2 \underline{x}} \int_V \left[\frac{\partial^2 p^{(o)}}{\partial t^2}\right]_{\hat{t}} dV(\underline{y})$$

In this case, the hydrodynamic pressure fluctuations $p^{(o)}$ of the turbulent flow can be considered as the basic source mechanism.

Both equation (2.5) and (2.6) are valid only in the geometric far field ($\underline{x} >> \underline{y}$) and the acoustic far field ($\underline{x} >> \lambda$). If the region of unsteady flow contains no surfaces then either equation should accurately describe the acoustic pressure received in the far field.

If a surface is imbedded in the turbulent flow, then an additional result due to Curle[2] must be considered. Again the isentropic assumption applies, and the far field approximation has been made;

$$(2.7)\quad P(\underline{x},t) = \int_S \left[\frac{\partial}{\partial t}(\rho u_n)\right]_{\hat{t}} dS - \frac{\partial}{\partial x_i}\int_S \left[\frac{P_i + \rho u_i u_n}{4\pi \underline{x}}\right]_{\hat{t}} dS - \frac{1}{4\pi c_o^2 \underline{x}} \int_V \left[\frac{\partial^2}{\partial t^2} p^{(o)}\right]_{\hat{t}} dV$$

$P_i = -l_j(p\delta_{ij} - \tau_{ij})$ = total force per unit area exerted on the fluid by the surface.

u_n = velocity component normal to the surface

The two surface integrals describe the additional radiated noise resulting from the interaction of the turbulence with the surface. If the surface is rigid ($u_n = 0$) and if shear stresses are small compared to normal stresses ($\tau_{ij} << p\delta_{ij}$), then equation (2.7) can take the reduced form:

$$(2.8)\quad p(\underline{x},t) \doteq \frac{1}{4\pi \underline{x} c_o}\int_S \cos\theta \left[\frac{\partial P_n}{\partial t}\right]_{\hat{t}} ds \; - \frac{1}{4\pi c_o^2 \underline{x}}\int_V \left[\frac{\partial^2 P^{(o)}}{\partial t^2}\right]_{\hat{t}} dV$$

P_n = pressure exerted on the surface by the fluid

θ = angle between a normal to the surface and the observer

2.2 Causality Source Location Technique

Traditionally, researchers have obtained estimates of the radiated acoustic intensity from each source region by squaring and time averaging* either equation (2.5) or (2.6), as done below to equation (2.5):

$$(2.9)\quad \overline{p(\underline{x},t)p(\underline{x},t')} \doteq \frac{1}{16\pi^2 \underline{x}^2 c_o^4}\int_V\int_{V'} \left[\frac{\partial^4}{\partial \tau^4}\left(\overline{\rho u_x^2 \rho u_x'^2}\,(\tau,\xi)\right)\right]_{\hat{t}-t'} d^3\xi\, d^3\underline{y}$$

The processes are assumed to be statistically stationary so that $\overline{p(x,t)p(x,t')}$ is only a function of $t-t'=\tau$. Two probes, each measuring momentum fluctuations in the direction of the far field microphone, are separated by all possible combinations of space separation (ξ) and time (τ). A two-fold integral over the correlation volume and the entire source region is necessary. Because of the enormous number of measurements required, and because it is necessary to take the fourth time derivative of each cross-correlation to finally get an estimate of $\overline{p(\underline{x},t)p(\underline{x},t')}$, the method has proven to be largely unsuccessful in obtaining detailed information about the spatial distribution of noise sources within jets.

---

* overbars denote time averages over a time period which is long compared with characteristic periods of p(t).

More recently, a much simpler but equivalent method of determining source strength and distribution has been used by Siddon[13], Meecham and Hurdle[8], Rackl[12] and others. Both sides of equation (2.6) (if the pressure source model is used) are simply multiplied by the sound pressure received in the far field.

(2.10) $$p(\underline{x},t)p(\underline{x},t') \doteq \frac{1}{4\pi \underline{x} c_o^2} \int_V \left[\frac{\partial^2 p^{(o)}}{\partial t^2}\right]_{t-t'-\underline{x}/c_o} dV(\underline{y}) \cdot p(\underline{x},t')$$

Taking a time average and assuming a statistically stationary process,

(2.11) $$\overline{pp}(\tau) \doteq -\frac{1}{4\pi c_o^2 \underline{x}} \int_V \left[\frac{\partial^2}{\partial \tau^2}\left(\overline{p^{(o)}p}(\tau)\right)\right]_{\tau-\underline{x}/c_o} dV$$

$\overline{pp}(\tau)$ is the self or "auto" correlation of the far field sound with itself. The contribution to $\overline{pp}(\tau)$ from a single element of source space is now proportional to the second time derivative of a single correlation. Thus it is dependent on only one inflow probe position, yet is exactly equivalent to equation (2.9). The far field intensity ($I=\overline{p^2}/\rho c$) results if τ is set equal to zero. Correspondingly, the cross-correlation function $\overline{p^{(o)}p}$ must be evaluated at retarded time $\tau = \underline{x}/c_o$. The intensity I from each noise source volume is a measure of the acoustic power flow from that source in a given direction, so that the source strength from a region in the jet can be written as:

(2.12) $$\frac{dI}{dV} = \frac{1}{\rho c_o}\frac{d\overline{p^2}}{dV} = -\frac{1}{4\pi\rho c_o^3 \underline{x}}\left[\frac{\partial^2}{\partial\tau^2}\overline{p^{(o)}p}(\tau)\right]_{\tau=\underline{x}/c_o}$$

A hypothetical correlation function is shown in Figure 4. Such

a smooth symmetric curve should be the result for pure jet noise with no surfaces interacting with the turbulence. However the correlation taken by Rackl (see Figure 1) is much different, indicating some additional surface effect.

The acoustic intensity received in the far field due to both volume and surface effects can be found by simply multiplying Curle's result (equation (2.8)) by $p(\underline{x},t')$.

$$(2.13)\quad p(\underline{x},t)p(\underline{x},t') \doteq \frac{-1}{4\pi c_o^2 \underline{x}} \int_S \cos\theta \left[\frac{\partial P_n}{\partial t}\right]_{\hat{t}-t'} p(\underline{x},t')\, ds - \frac{1}{4\pi c_o^2 \underline{x}} \int_V \left[\frac{\partial^2}{\partial t^2} P^{(o)}\right]_{\hat{t}-t'} p(\underline{x},t')\, dV$$

Again assuming stationarity and time averaging,

$$(2.14)\quad \overline{pp}(\tau) \doteq \frac{-1}{4\pi \underline{x} c_o} \int_S \cos\theta \left[\frac{\partial \overline{P_n P}}{\partial \tau}\right]_{\tau-\frac{\underline{x}}{c_o}} ds - \frac{1}{4\pi \underline{x} c_o^2} \int_V \left[\frac{\partial^2}{\partial \tau^2} \left(\overline{P^{(o)} P}\right)\right]_{\tau-\frac{\underline{x}}{c_o}} dV$$

For researchers using the causality technique, it has been common to measure the correlation $\overline{p^{(o)}p}$ and assume that the unwanted portion $\overline{p_n p}$ will be small. It is certainly true that the total intensity sensed in the far field will almost exclusively be due to the jet turbulence. However, the pressure of the surface can still seriously contaminate the correlation between local jet pressure and far field sound if the probe surface is comparable in size to the correlation volume of the adjacent turbulent "eddies". Unfortunately, this is likely to be true for most model

jet experiments (the contaminating effect is described theoretically in section 4). Other than reducing the probe size, only three alternatives appear available to reduce the effect of a pressure probe on the jet pressure-far field correlation.

i) Because the surface term has a directivity described by $\cos\theta$, if the far field microphone is situated so that $\cos\theta \longrightarrow 0$ then the contribution from the surface will not be included in the correlation.

ii) Since the surface term is dipole in nature, the noise which it produces will be proportional to V_{jet}^{6}. The jet noise however, is known to vary roughly as V_{jet}^{8}, so that the relative contribution of the probe noise should be less at higher speeds.

iii) In some cases it may be possible to separate the effects of the probe noise from the jet noise, as they may occur at different delay times on the correlation function.

3. PHYSICAL MODEL OF CONTAMINATION

To understand the process of probe noise contamination, we consider the case of a probe imbedded in a turbulent flow and aligned with the flow as shown in Figure 2. Although turbulence can really only be characterized by statistically determined structures, for simplicity we will consider the flow to be made up of discrete turbulent "eddies".

If we imagine such an eddy at position 2 on the probe, the pressure fluctuations within the eddy will be sensed by the probe, and assuming proper probe design, can be assumed to be within 20% of the true pressure fluctuations.* As a by-product of these violent inertial fluctuations, there will be much smaller acoustic waves generated, travelling away from the source region, arriving at the far field microphone at a time $\hat{t}$ later. The strongest correlation between the far field and the probe should result therefore, if the probe signal is delayed by time $\hat{t}=\underline{x}/c_o$ relative to the microphone signal. If the probe is aligned with the time averaged flow, there will be only negligible lift or side forces acting in the vicinity of the pressure tap. Considerably higher forces will occur however, at the tip and stem of the probe. These are in the form of fluctuating lift or side forces at the tip, and predominantly drag forces on the stem. Also, any points on the probe where area changes occur will lead to fluctuating surface forces (and to separation if the area change is sudden). As a result, these areas on the probe will also be acoustic emitters, radiating additional noise which would not have existed

---

* see Appendix B

without the probe being present and which will be sensed by the far field microphone. This does not mean that the far field pressure spectrum will be significantly altered, nor that the overall far field sound will be increased very substantially, since it will include noise coming from the entire jet and all other uncorrelated eddies. Nevertheless, the unwanted probe noise may be appreciable or even greater than the noise produced by the jet turbulence within one correlation volume. Furthermore, the probe noise will often have very similar spectral properties to the legitimate jet noise.

The noise from the probe tip and stem will not correlate at exactly the same time as the jet noise. To understand this, consider the following: if in fact we wanted to get the correlation between the probe noise and the far field pressure we can do it two ways. First, we could simply move the pressure measuring holes to the tip, so that the tip pressures would correlate with the far field microphone at some time t later, dependent on the sound speed and distance to the far field microphone. Now note that the pressures sensed at the tip will be the sum of the legitimate jet pressures and the additional tip pressure distribution due to lift and side forces; hence the correlation due to probe noise would be exactly superimposed on the jet pressure correlation. An alternative method to get the probe noise-far field correlation would be to leave the holes at point 0 (in Figure 2), and assume that the turbulent jet pressures which occurred at the tip will be the same as at point 0. Since the distance is short, this is reasonably accurate if the convecting turbulent field is changing slowly. As the pressure fluctuations must convect at a

velocity U_c over a distance Y_t from the tip to the sensing holes, then an acoustic signal due to the interaction of the turbulence with the tip will leave the probe at a time $\Delta t \simeq Y_t/U_c$ before the pressure fluctuations in the turbulence are sensed by the probe at point 0. Consequently, a strong correlation will occur at time $\hat{t}-\Delta t$ due to the probe tip noise, as well as a strong correlation at time $\hat{t}$. In both cases the far field microphone is correlating with the same turbulent "eddy".

Now in fact we do not want to correlate the probe tip noise with the far field, but this happens naturally because the velocity field which produces probe noise is also generating legitimate jet noise of similar character. Thus there appears an additional bump on the correlation due to tip noise before the correct time delay and an additional bump due to stem noise after the correct time delay.

If Δt is large enough, then it may be possible to completely separate the contaminating correlation from the jet pressure correlation. Since the real jet pressure correlation is often very much smaller than the probe noise correlation, any overlap between the two correlations can obscure the true jet pressure correlations completely. Before quantitative source strength analysis can be done it is necessary to know the magnitude of error in the cross-correlation and if, indeed, the legitimate source-far field correlation can ever be detected accurately.

4. ANALYTICAL MODEL

A primary purpose here is to theoretically predict the shape of the causality correlation function which will occur, including the contamination effects of an inserted probe. The geometry associated with the problem is shown in Figure 5. Details not given here appear in Appendix A.

The correlation function $\overline{pp^{(o)}}(\tau)$ is the time averaged product of the jet (source) pressure $p^{(o)}$ and the corresponding far field acoustic pressure p. The relation describing this function is obtained in a manner analogous to the derivation of the causality integrals (equation (2.14)). In the present case however, we multiply both sides of the radiation equation (equation (2.8)) by the source jet pressure before time averaging. Again assuming the turbulence to be statistically stationary the following relation results:

$$(4.1)\qquad \overline{P P^{(o)'}}(\tau) \doteq \underbrace{\frac{-1}{4\pi x c_o}\int_S \cos\theta\left[\frac{\partial}{\partial\tau}\overline{P_n P^{(o)'}}\right]_{\tau-\frac{x}{c_o}} ds}_{I_1} - \underbrace{\frac{1}{4\pi x c^2}\int_V \left[\frac{\partial^2}{\partial\tau^2}\overline{P^{(o)} P^{(o)'}}\right]_{\tau-\frac{x}{c_o}} dv}_{I_2}$$

$p^{(o)'}$ = pressure measured by the probe. For a well designed probe in quasi-steady flow, this will closely approximate the true jet pressure.

$p^{(o)}$ = the real jet pressure

p = far field pressure

It can be seen that the shape of $\overline{pp^{(o)'}}(\tau)$ depends on two terms. The first is the surface integral of the cross-correlation between the probe detected jet pressure $p^{(o)'}$ and the local surface pressures P_n measured at all other points on the probe surface S. This term represents the unwanted portion of the correlation due to the probe surface noise. The second term is a volume integral of cross-correlations between $p^{(o)'}$ and the corresponding true jet pressures $p^{(o)}$ measured at all other points in the adjacent regions of turbulence. This is the correlation resulting from legitimate jet noise.

In order to model the contaminated correlation between the far field pressure and the source jet pressure, it is necessary to estimate integrals I_1 and I_2. It is known that turbulent eddies exhibit the properties of convection and decay with space and time, so that in theoretical predictions of noise generation by turbulence, it has been common to assume a convecting Gaussian function for $\overline{p^{(o)}p^{(o)'}}$:

$$\overline{p^{(o)}p^{(o)'}}(\tau) = \overline{p^{(o)^2}}\, e^{-\frac{(y_1 - U_c\hat{\tau})^2}{L_1^2} - \frac{y_2^2}{L_2^2} - \frac{y_3^2}{L_3^2} - \frac{\hat{\tau}^2}{T^2}} \tag{4.2}$$

where U_c = convection speed of the eddies

L_1, L_2, L_3 = integral length scales of the turbulent eddies: L_1 being in the direction of the flow while L_2 and L_3 are transverse to the flow.

T can be considered a typical lifetime of a turbulent eddy. The decay parameter $\hat{\tau}/T$ must be non-zero, in order that the flow may generate sound.

Substituting (4.2) into I_2 and integrating with limits at infinity yields the following solution:

$$(4.3) \qquad I_2 = \frac{\overline{p^{(0)^2}} L_1 L_2 L_3 \sqrt{\pi}}{2 c_0^2 \bar{x} T^2} \left[e^{-\frac{\hat{\tau}^2}{T^2}} \left(1 - 2\frac{\hat{\tau}^2}{T^2}\right)\right]$$

which predicts a symmetrical curve as shown in Figure 6. The correlation should peak at a time delay $\tau = \bar{x}/c_0$ corresponding to the necessary acoustic travel time for a pressure disturbance in the source region to reach the far field microphone.

Integral I_1 can be written in the equivalent form below (see Appendix A):

$$(4.4) \qquad I_1 = \frac{\cos\beta}{4\pi \bar{x} c_0} \int_{-\infty}^{y_{tip}} \frac{\partial}{\partial \tau} \left(\overline{p^{(0)} f}\right) dy'$$

where f is the net side force per unit length on the probe in the plane of the far field microphone, and β (see Figure 5) is the angle between the force vector and the far field microphone. The integral over y' extends from $-\infty$ to the probe tip since we imagine the probe to extend indefinitely downstream after the pressure measuring taps. This simply means that sources of contamination which occur after the pressure taps (due to drag forces on the stem or to sudden area changes) will not be modelled here. This situation was duplicated experimentally by extending the pressure taps a considerable distance in front of the supporting stem so that contaminations which occur because of downstream anomalies will appear later in time on the correlation signature than the "true" pressure correlation. For the probe shape being modelled here, the form chosen for

$\overline{p^{(o)'} f}$ is:

$$(4.5) \qquad \overline{p^{(o)'} f} = \underbrace{CR}_{D}\underbrace{K(Y_{TIP}-y')\, e^{-\frac{(Y_{TIP}-y')}{kd}}}_{C} - \underbrace{\frac{(y'+U_c\hat{\tau})^2}{L_1^2}}_{B} - \underbrace{\frac{\hat{\tau}^2}{T^2}}_{A}$$

The various terms in this empirical form are explained as follows:

A: As in the jet pressure correlation, this term describes the expected decay of turbulence with time. T is a typical time scale for decay in the convecting frame of reference.

B: This describes the convection of the turbulence in the y' direction and its decay with distance. L_1 is the streamwise correlation length.

C: This is a weighting function for the correlation which approximates the expected side force distribution on the probe. It is sketched approximately in Figure 6. The constant k determines the distance from the probe tip where the side force distribution is expected to peak. For this work we have assumed f_{max} to occur at a distance ½ diameter from the probe tip, which requires that k=½. The exact distance depends upon the precise probe tip geometry, but for any round-nosed axisymmetric body the peaking distance is not likely to be greater than one diameter, or less than 1/8 diameter. K is a parameter which governs the magnitude of the side force distribution, and can be calculated if the total side force

resulting from cross flow (due to incidence changes) is known:

$$F_{TOTAL} \doteq \frac{1}{2}\rho U_c^2 \frac{dC_L}{d\alpha} \cdot \alpha \cdot \text{AREA} = \int_{-\infty}^{Y_T} K(Y_T - y') e^{-\frac{(Y_T - y')}{kd}} dy'$$

Assuming* $\frac{dC_L}{d\alpha} = 2$; $\alpha \simeq \frac{v'}{U_c}$; Area $\simeq \frac{\pi d^2}{4}$ and integrating, gives $K = \frac{\pi\rho v' U_c}{4k^2}$.

v' is the root-mean-square value of the cross-stream turbulence velocity.

D: R is a parameter which must have units of pressure. To a first approximation, R is assumed to equal the root-mean-square pressure at the point of measurement (i.e.$\simeq .05\frac{1}{2}\rho V_j^2$ at $x_o=4D$, $y_o=\frac{1}{2}D$). C is a coupling coefficient which attempts to describe the coherence between probe side force f and jet pressure $p^{(o)'}$ when $\hat{\tau}=0$ and $y'=0$. If the correlation were perfect, C would equal 1. Since no information is available on the expected correlation between f and $p^{(o)'}$, C was left to be fitted to the experimental results. For C to equal 1 would imply an identical phase and amplitude variation for f and $p^{(o)}$. Although some degree of coherence is to be expected between side force (proportional to v'/U_c) and the local jet pressure, it is extremely unlikely that a perfect one-to-one compatability exists.

If the function for $\overline{p^{(o)'} f}$ given in equation (4.5) is substituted into I_1 of equation (4.1) the following integral results:

$$(4.6) \qquad I_1 = -\frac{\cos\beta\, CRK}{4\pi C_o \Sigma} \int_{-\infty}^{Y_T} (Y_T - y') e^{-\frac{(Y_T - y')}{kd} - \frac{(y' - U_c\hat{\tau})}{L_1^2} - \frac{\hat{\tau}^2}{T^2}} dy'$$

where $$CRK = \frac{C\pi}{8k^2}\left(\rho_j V_j^2\right)^2 \left(\frac{U_c}{V_j}\right)^2 \frac{p^{(o)}}{\frac{1}{2}\rho_j V_j^2} \left(\frac{v'}{U_c}\right)$$

---

*These are reasonable values for a slender axisymmetric body subjected to small, quasi-steady incidence changes.[7]

Therefore by solving I_1, and combining with the solution for I_2, we get the contaminated correlation function:

$$(4.7)\quad \overline{P^{(o)}P(\tau)} = \frac{\cos\beta\, C}{32 k^2 \underline{x} c_o}(\rho_j V_j^2)^2\left(\frac{U_c}{V_j}\right)^2\left(\frac{p^{(o)}}{\frac{1}{2}\rho_j V_j^2}\right)\left(\frac{v'}{U_c}\right)e^{-\frac{\hat{\tau}^2}{T^2}}$$

$$e^{\frac{2}{kd}\left(\frac{L_1^2}{2kd} - U_c\hat{\tau} - Y_T\right)}\operatorname{erfc}\left(Q/L_1\right)\left\{\left(\frac{\hat{\tau}L_1^2}{U_c T^2} + U_c\hat{\tau} + Y_{TIP}\right)U_c L_1\sqrt{\pi}\right.$$

$$\left. + \frac{U_c Q e^{-\frac{Q^2}{L_1^2}}}{\operatorname{erfc}(Q/L_1)} - U_c\sqrt{\pi}\left(\frac{Q^2}{L_1} + \frac{L_1}{2}\right)\right\}$$

$$+ \frac{\overline{P^{(o)2}}\, L_1 L_2 L_3\sqrt{\pi}}{2c_o^2 \underline{x} T^2}\left\{e^{-\frac{\hat{\tau}^2}{T^2}}\left(1 - 2\frac{\hat{\tau}^2}{T^2}\right)\right\}$$

where $\quad Q = \frac{L_1^2}{kd} - U_c\hat{\tau} - Y_t$

For the position where turbulence is highest in a round subsonic jet (i.e., $x_o/D=4$ and $y_o/D=\frac{1}{2}$), the flow parameters have the following nominal values[9]:

$$\frac{U_c}{V_j} \simeq .6 \qquad L_1 = .4D$$

$$\frac{p^{(o)}_{rms}}{\frac{1}{2}\rho_j V_j^2} \simeq .05 \qquad L_2 = L_3 = L_1/3$$

$$\frac{v'}{U_c} \simeq .20 \qquad {}^{10}T = \frac{2.2\ D}{V_j}$$

At other points in the jet the flow parameters will be different, but the form of the function will be similar. I_1 predicts a relatively

antisymmetric curve as shown in Figure 6 with a maximum slope occurring at a time Y_{peak}/U_c before the correct time delay. I_2 predicts a symmetric curve also shown in Figure 6 which has zero slope at the correct time delay, $\hat{\tau} = 0$.

5. EXPERIMENTAL APPARATUS

The purpose of the experimental investigation undertaken was to confirm the general characteristics of the correlation model. This consists of two objectives; first, to confirm the shape of the modelled function, and second, to discover whether those parameters on which the empirical correlation function depends do indeed have the predicted effect. Probes of varying sizes were built to test the change in contamination resulting from size changes. Each of the probes were tested at Mach numbers ranging from .35 to .83 to determine the change in contamination with velocity.

5.1 Jet Facility

A rotary compressor rated at 280 cfpm (.132 m^3/second) of standard air was available for use. Air pressure delivered was 100 psi (690 KPa). With our 2 cm diameter jet this has a capability to run continuously at M=1. For higher velocities, the rig must be run in a blow-down mode, for which a large 1.9 m^3 receiver is available. While the jet is running at lower velocities the receiver also serves to effectively damp out possible pressure surges caused by the compressor during start-up and shut-down. A Fisher pressure regulator was used to control the flow rate at all Mach numbers. The flow rate was monitored by both a water manometer for low velocities ($M \leq .35$), and a mercury manometer for higher velocities. Both manometers could be read to an accuracy of $\pm$ 1 mm.

Approximately 5 minutes was required for the system to reach equilibrium, after which the flow rate was remarkably stable. A silencer was placed between the control valve and the jet plenum in order to eliminate upstream valve noise. This consisted simply of loosely rolled fibreglass in an enlarged pipe section. An 8 cm flexible hose was used between the control valve and the jet plenum to further reduce upstream noise due to sharp pipe bends and fittings. With the jet nozzle removed, the upstream valve noise could not be detected with a B&K ½" microphone when the chamber door was closed. The chamber was exhausted through a perforated section of the main door, positioned downstream of the jet axis.

The jet plenum design is shown in Figure 7 . The plenum consists of three sections;

i) a fibreglass lined section to further reduce noise and to encourage the jet entering the plenum to diffuse quickly.

ii) screens and honeycomb for flow straightening

iii) a short settling section so that those small eddies generated at the screens and honeycomb can be damped out.

The maximum velocity (at M=.83) in the settling chamber is extremely low (1.8 m/sec) so that the approach flow is essentially laminar.

The nozzle used (see Figure 8) was designed to give a uniform velocity profile at the exit plane (Smith and Wang)[19]. A plot of the mean velocity across the exit plane is given in Figure 9 . The large contraction ratio (156:1) ensures very thin boundary layers and a low turbulence level.

A special traversing mechanism was designed to minimize the surface area in close proximity to the jet. This is shown in Figure 10. The objective was to eliminate any undesirable acoustic reflections which might further contaminate the correlation function. The traverse gear is capable of radial and axial movement over the significant regions of jet turbulence, and is accurate to ±.5 mm.

5.2 Instrumentation

The far field microphone was a ¼" B&K type 4135. This has a flat frequency response up to 40 kHz and a maximum phase shift of 35° at 40 kHz. The output from this microphone was amplified, filtered and fed into a Saicor Model 43A signal correlator, channel B. A schematic of the signal path is shown in Figure 11.

The in-flow probe consisted of a .030 in. (.078 cm) diameter Kulite semiconductor pressure transducer, imbedded inside static pressure sleeves of three different sizes. As shown in Figure 12, a section of hypodermic needle was used as a fixed Kulite holder, so that different probe sizes could be tested without constantly disturbing the Kulite transducer. The stem of the probe was airfoil shaped in order to reduce the drag fluctuations and to increase the stem stiffness in the axial direction.

The Kulite transducer was calibrated using a 250 Hz pure tone, and the sensitivity was found to closely match the manufacturer's specifications. The signal from the Kulite was amplified, filtered (20 Hz - 40 kHz) and fed into channel A of the Saicor correlator.

Because the size of the sensing diaphragm on the Kulite transducer is very much smaller than the smallest wavelength to be measured, all of the frequencies of interest will appear to the diaphragm as spatially uniform pressure waves. As a result, no high frequency roll-off is expected, so that a frequency response calibration for the Kulite transducer was felt to be unnecessary. Since the phase shift is related to the frequency response, it also is expected to change very little up to the maximum frequency of interest.

When the hypodermic tubing containing the Kulite is inserted into the static pressure sleeves, a small cavity is formed directly before the Kulite diaphragm, which could lead to a resonant condition at the Helmholtz frequency of the cavity. To avoid this, the cavity size for each probe was kept as small as possible so that resonance was forced to occur above 40 kHz.

To concur with the quasi-steady assumption of section 4, the diameter of the static pressure sleeves must be small compared to the expected correlation scales. At $x_o/D=4$ and $y_o/D=\frac{1}{2}$, a typical streamwise velocity scale would be about $.1x_o$ (.8 cm) and about $.04x_o$ (.32 cm) in the transverse direction. The largest probe used is .470 cm in diameter and does show a slightly lower overall rms pressure than the smaller probes, indicating some loss of high frequency information due to its poorer spatial resolution.

For accurate pressure measurements in steady flow using a standard probe, it is necessary to locate the pressure taps about 6

diameters downstream from the nose and about 8 diameters upstream from the stem in order to cancel the tip and stem effects. For unsteady flow, the pressure taps should be located in a similar position in order to be insensitive to streamwise velocity fluctuations. Since all three of the static pressure sleeves are the same length (see Figure 13) it was necessary to place the pressure taps for the largest probe at a distance only a little greater than 4 diameters from the nose. Referring to Figure 14, it can be seen that for steady flow, such placement will lead to only a slightly larger error.

A 1/8" B&K microphone was used as an in-flow probe for a portion of the experimental work in order to demonstrate the effect on the cross-correlation signature of changing the probe nose length. To simulate a long probe, a dummy nose piece was glued onto the grid cap as shown in Figure 13. For a short probe, a standard B&K nose cone was used, also shown in Figure 13.

A Plotamatic x-y recorder was used to plot the correlation functions. Autocorrelations were taken in order to non-dimensionalize the cross-correlations with the autocorrelation values at $\tau=0$. The autocorrelation of the in-flow probe was also a convenient check for cavity resonance or probe vibration. Probe vibration can be detected since any resonant movement of the probe would be sensed by the probe as a regularity in the flow, resulting in a periodic autocorrelation function. This became a problem only for the largest probe while operating at the highest Mach number (M=.83) so that results for this condition are not reported.

6. EXPERIMENTAL RESULTS

As discussed in section 4, an analytical model has been developed which is expected to predict the effect of probe noise on causality cross-correlations. For a standard probe with a long nose, the portion of the cross-correlation due to probe tip noise is predicted to have a maximum slope at a time before the legitimate jet pressure correlation, given by the distance Y_{peak} and the convection velocity U_c (see Figure 6). The first experiments, therefore, were intended primarily to confirm the existance of probe tip noise, and its dependence on probe length for its time of occurrance on a cross-correlation.

If different probe diameters and a variety of Mach numbers are used as inputs to the analytical model, certain functional relationships will exist between these variables and the degree of contamination. A second set of experiments was carried out to test the predicted relationships.

6.1 Bruel and Kjaer Microphone Experiments

Since many experimenters use standard B&K microphones with attached nose cones as probes for cross-correlations, it was decided to duplicate this set-up using a 1/8" B&K microphone. A symmetrical airfoil was glued onto the microphone preamplifier (see Figure 13) in order to reduce the drag resulting from the jet flow. The diaphragm of the

microphone was placed at a position $x_o/D=4$ and $y_o/D=\frac{1}{2}$. The far field microphone was situated perpendicular to the jet, so that cos β in equation (4.6) will equal unity. In this position only the side force fluctuations on the probe tip should contribute noise to the far field microphone (drag force fluctuations on the stem will radiate in the upstream-downstream direction). The experimental result is plotted in Figure 15, and appears much like legitimate jet noise, having an almost symmetrical shape at the correct time delay. Also plotted in Figure 15 is the analytical result. This was evaluated using the expression for the jet noise correlation as it appears in equation (4.3) and adding to it a numerical integration of the probe noise correlation term as it appears in equation (4.6). A best fit was obtained by assigning a value .50 to the coupling coefficient C (explained in D following equation (4.5)). If a constant convection velocity is assumed over the length of the probe, then the time scale on the cross-correlation function can be converted to a length scale on which a sketch of the in-flow probe can be superimposed with the pressure taps corresponding to $\hat{\tau}=0$. If this is done, anamolies on the correlation function can be projected downward to regions on the probe sketch from which the anomalies occurred.

Most of the peak in the predicted correlation curve at $\hat{\tau}=0$ is due to the sharp rise in pressure near the front of the nose cone. The resulting probe noise occurs just before the correct time delay but causes a peak at the correct time delay. The true jet pressure correlation appears as a broader and shorter hump, but is almost completely masked by the probe noise correlation.

The shape of the experimental curve agrees well with the analytical result except for a large bump after $\hat{\tau}=0$. The superimposed probe sketch clearly suggests that this anomaly is due to the change in cross-sectional area which occurs along the probe. Since only probe tip noise has been modelled as a source of contamination, no such bump occurs on the analytical curve.

If a B&K microphone modified as in Figure 13 is inserted into the flow (again at $x_o/D=4$, $y_o/D=\frac{1}{2}$), then the long probe tip should ensure that the probe noise from the tip will be well separated in time from the true jet pressure correlation. Both the experimental and the analytical results are plotted in Figure 16. The coupling coefficient C was left unchanged from the previous experiment. As predicted, the probe noise portion of the correlation does appear to occur at nearly the expected time delay Y_{peak}/U_c.

The predicted jet noise correlation appears as a broad hump in the analytical curve, and is now clearly visible. There does not appear to be any experimentally observed counterpart to the predicted jet noise correlation. The bump on the experimental curve which occurs directly after $\hat{\tau}=0$ is likely due to the sharp discontinuity on the probe surface where the grid cap ends. This same noise source was probably also active in the previous experiment (due to separation from the nose cone cap) although its presence may have been masked by the very large tip noise peak which occurred at $\hat{\tau}=0$.

A comparison of Figures 15 and 16 clearly demonstrates the dependence of causality correlations on tip distance, and confirms the existance of probe noise as a significant contaminant of the correlation function. Since the use of B&K nose cones for pressure correlations in model jets is quite common, our findings suggest the possibility that many researchers have been measuring mostly probe noise and very little legitimate correlation from the turbulent sources.

6.2 Normalizing Procedure

It is perhaps necessary at this point to explain the normalizing procedure used in presenting the data. The most common procedure in normalizing cross-correlations is to divide the time-averaged product by the rms values of the two fluctuating variables being correlated, as in equation (1.1): $\overline{PP^{(\omega)}}/\left(\sqrt{\overline{p^{(\omega)2}}}\sqrt{\overline{P^2}}\right)$. Such a procedure however, does not clearly show the effect of probe size or Mach number on the cross-correlation. Furthermore, it does not provide a means of extrapolating to other experimental combinations of probe size, jet diameter, Mach number or far field distance. In the present case, the pressure p received in the far field due to a single turbulent source is estimated from equation (2.6):

$$p(\underline{x},t) = \frac{-1}{4\pi C_o^2 \underline{x}} \int_V \left[\frac{\partial^2}{\partial t^2} p^{(\omega)}\right]_{\hat{\xi}} dv(\underline{y})$$

For one noise source the integral is only over one correlation volume, but .

for the entire jet (which is what our far field microphone measures) the integral must include the entire jet volume. The far field pressure from the entire jet can be considered to vary therefore, as follows:

$$P \propto \frac{1}{x c_o^2} \frac{\partial^2}{\partial t^2} p^{(o)}(V) \qquad V = \text{entire jet volume}$$

If the following dimensional approximations are made,

$$V \sim D^3$$

$$\frac{\delta}{\delta t} \sim \frac{V_j}{L}$$

$$L \sim D$$

D = jet diameter

L = turbulent length scale

then $P \propto \frac{p^{(o)'}}{x c_o^2}\left(\frac{V_j}{D}\right)^2 D^3$. The pressure $p^{(o)'}(\simeq p^{(o)})$ measured by the probe will be some fraction of the available dynamic head, $p^{(o)'} \sim \rho_j V_j^2$. If the expressions for $p^{(o)'}$ and p are substituted into the classically normalized cross-correlation function, the following results:

$$(6.1) \quad \frac{\overline{P p^{(o)'}}}{\sqrt{\overline{P^2}}\sqrt{\overline{p^{(o)'2}}}} \sim \frac{\overline{P p^{(o)'}}}{(\rho V_j^2)^2 M_j^2 \frac{D}{x}} = C_m(\tau)$$

This last form reflects the normalizing procedure used to present all of the data, and enables easy scaling from one experimental set-up to another. The following dimensionless formula should also be useful:

$$C_m\left(\frac{U_c \hat{\tau}}{Y_t}\right) \doteq \frac{\overline{P p^{(o)'}}\left(\frac{U_c \hat{\tau}}{Y_t}\right)}{(\rho V_j^2)^2 M_j^2 \frac{D}{x}} = f\left(\frac{d}{D}, M_j, \text{PROBE SHAPE}\right)$$

6.3 Parametric Investigations

It is possible to get rough approximations of the effect of probe diameter and Mach number on the function $\frac{\overline{pp^{(o)'}}}{(\rho_j V_j^2)^2 M_j^2 \frac{D}{x}}$ if dimensional estimates of p and $p^{(o)'}$ are made. If the sound received in the far field from a single coherent region is dominated by the probe noise, then equation (2.8) predicts that

$$\underset{\substack{\text{far field}\\(\text{Probe noise})}}{P(x,t)} = \frac{-1}{4\pi x c_o}\int_S \cos\theta\left[\frac{\delta P_n}{\delta t}\right] ds \qquad \text{or } p(\underline{x},t) \sim \frac{1}{\underline{x}c}\frac{\delta}{\delta t} P_n \cdot A$$

where A equals the correlation area over the probe surface. Again making dimensional approximations:

$$\frac{\delta}{\delta t} \sim \frac{V_j}{L}$$

$L \sim D$ (at a particular x_o/D, y_o/D)

P_n is the surface pressure on the probe and will be some fraction of the available dynamic head $\sim \rho_j V_j^2$

$$A \sim d^2$$

$$p^{(o)'} \sim \rho_j V_j^2$$

Substituting into equation (6.1);

$$(6.2)\quad \frac{\overline{PP^{(o)'}}}{(\rho_j V_j^2) M_j^2 \frac{D}{x}} \sim \frac{\frac{1}{xc}\frac{V_j}{D}(\rho V_j^2)^2 d^2}{(\rho V^2)^2 M_j^2 \frac{D}{x}} = \left(\frac{d}{D}\right)^2 \frac{1}{M_j}$$

We expect therefore, the normalized cross-correlation coefficient

of the probe noise to vary as $\left(\frac{d}{D}\right)^2 \frac{1}{M_j}$. The portion of the correlation due to pure jet noise however, would not be expected to vary at all, unless the degree of coherence in the jet is itself a function of Mach number.

As shown in Figure 13, three static pressure sleeves were built for the Kulite transducer, all about the same length ($Y_t \simeq 1.91$ cm) but with different d/D ratios (i.e., .118, .159 and .236). The three different probes were used for cross-correlations with the far field microphone at four different jet Mach numbers (i.e., .35, .51, .68 and .83). In each case, the pressure taps were placed in the jet at $x_o/D=4$, $y_o/D=\frac{1}{2}$ as before. The experimental results for each Mach number are plotted uppermost in Figures 17 to 20, with predicted curves plotted below in each case. The predicted curves were generated exactly as in the previous section, using the closed form solution for the jet noise given in equation (4.3) and adding to it a numerically integrated result of the probe noise as given in equation (4.6).

The predicted increase in contamination with diameter appears somewhat stronger than that observed experimentally. In Figure 21, the log of the maximum values of the normalized cross-correlation function ($C_{m_{max}}(\tau)$) is plotted at a constant Mach number against the log of all three d/D ratios. It is evident that the predicted variation follows a $\left(\frac{d}{D}\right)^2$ law (this was expected, given by equation (6.2)) while experimentally we observe a $\left(\frac{d}{D}\right)^{1.45}$ law. This discrepancy is possibly because the expression for $p^{(o)'}f$ in the analytical model implicitly assumes quasi-steady conditions regardless of probe size. Since the transverse

length scale of the turbulent velocity field* is about .3-.4 cm, the ratio of eddy size to probe diameter approaches unity for the largest probes. Thus a quasi-steady side force model (as in Appendix A) will increasingly overestimate the actual forces produced as the probe size increases, relative to the eddy size.

For all of the predicted curves, the coupling coefficient C was assigned a value = .36. This gives a good fit to the experimental result with the smallest d/D ratio at the lowest Mach number, but increasingly underestimates the experimental results at higher Mach numbers. A plot of log $C_{m_{max}}(\tau)$ versus log [Mach number] at a constant d/D ratio (Figure 22) shows that the analytical results follow a $M^{-1.12}$ law while the experimental curves show no clear variation with Mach number. This could be because the coupling coefficient was assumed to be a constant, whereas it may vary with Mach number if the tip forces and measured pressures are better correlated at higher velocities. It is also a possibility that the turbulent length scales or intensities are changing, since any increase in these quantities with increasing Mach number would tend to overestimate the probe noise correlation at higher Mach numbers. This problem deserves further investigation.

6.4 Other Sources of Contamination

Although only the contamination due to the side forces on the probe tip has been discussed in this work, there are in fact, several other possible sources of correlated probe noise. The mechanisms for these, and

---

* based on velocity correlation measurements; the pressure scales could be as much as twice as large, based on Planchon's work.[10]

their expected directivity patterns are illustrated approximately in Figure 23. The resulting composite cross-correlation function is shown (hypothetically) near the bottom of the figure. The dominant effects are due to drag fluctuations on the supporting stem and local separation points at sharp corners, particularly near the elbow of the probe holder. The drag-induced dipole was not noted unless the far field microphone was placed at shallow angles to the jet centreline (i.e., for $\beta \longrightarrow 90^{\circ}$). A huge lift-induced contaminant was detected from the airfoil stem if the far field microphone was placed vertically above the probe in the direction of the lift fluctuations. A considerably larger source of contamination than expected occurred from the change in area as the pressure sleeves meet the airfoil stem. Fairing or smoothing at this point would only partially eliminate this source, although the largest probe, which has a diameter close to the thickness of the airfoil stem, showed less contamination.

Any cylindrical body in pure cross-flow will experience side forces associated with the circumferential pressure distribution, so that even at the pressure taps, small fluctuating side forces may pose a source of yet another, although probably weak, contamination.

Many of these other contaminant mechanisms are also amenable to empirical predictions, using a turbulence interaction model analogous to the fluctuating nose force model used here. A model describing the drag-induced contaminant on the stem for example, will be almost identical except that an appropriate weighting function which closely approximates the expected fluctuating force distribution due to drag will be necessary.

7. CONCLUDING DISCUSSION

The significant finding of this work is that probe noise has a strong influence on pressure correlations with the far field. It is evident that most conventional in-flow pressure probes will not provide useful correlations with the far field, so that probably probe noise, and not true turbulence noise, has been dominant in most of the previous causality experiments on jets. True jet noise correlations, if normalized, should be mainly a function of probe position and must not depend on such probe parameters as diameter or geometry. Some Mach number dependence is possible if the number of jet noise sources increases or decreases with Mach number. In any event, no clearly identifiable correlation with the far field due to jet noise has been observed in the experiments reported here. This was unexpected, and leads to the idea that the degree of coherence in the source region may be extremely weak. The results here indicate that the maximum correlation coefficient C (equation 1.1) must be smaller than .015 (based on the smallest value of d/D), suggesting about 5000 separate and uncorrelated regions of turbulence (see section 1.2). This is somewhat consistant with findings by Lee & Ribner[6] using a hot-wire. Previous correlation coefficients of order .1 (when using pressure probes) lead to an estimate of about 100 uncorrelated sources.

Since no definite indication of "true" jet source strength was

noted, it has not been possible to experimentally determine a suitable d/D ratio where tip-induced probe noise can be guaranteed to be less than the legitimate correlation. The curves resulting from the analytical model indicate that only at the smallest d/D ratio (.118) was $C_{m_{max}}$ ever equal to, or less than, the predicted jet noise. This is only an approximate result since the magnitude of the predicted probe noise correlations depends on the choice for the coupling coefficient C. For best fit, C does not vary substantially with diameter (within the limits of the quasi-steady model) but varies by a factor of about 2 over the range of Mach numbers tested.

Although the analytical model has been tested at only one point in the jet ($x_o/D=4$, $y_o/D=\frac{1}{2}$) and for only one probe geometry, the method is probably quite general. The particular point chosen is considered to be a region of dominant noise generation in subsonic jets, but the model is flexible enough so that contamination estimates could be made for other points in the jet using the appropriate measured values of the turbulence parameters.

The shape and parametric dependence of the probe noise correlation is reasonably well predicted by the model presented here, although some discrepancies do exist. It is surprising in fact, that the experimental trends have been reflected so well, if we consider some of the imperfections of the model: turbulence is not Gaussian, yet a Gaussian model has been used for both the probe noise correlation and the jet noise correlation. Furthermore, the estimates for the length scales in the

turbulence are based on an experimental fit to a space correlation function, while the convected time scale estimate is based on a similar fit to the envelope of space-time correlations. Neither function is actually exponential, and in both cases an exponential fit will be inadequate for high frequencies. For the time scale estimate the fit is also typically poor at low frequencies. In most cases, these estimates are based on hot wire measurements of the velocity field in very low speed jets (although the value used for the convected time scale here is based on pressure measurement[10], but at a very low Mach number), but there is evidence that length scales based on pressure are somewhat larger than those based on velocity. Measurements in higher speed flows may also indicate changes in these values. Aside from the crude estimates used for the turbulence parameters, the model must also be content with only a rough estimate of the true force distribution on the probe tip, as well as an arbitrary selection of the distance from the tip at which the distribution peaks.

In view of these imperfections, it is encouraging that the major features of the correlation functions are followed so well. Further development will lead hopefully, to a useful research tool which will quantify accurately the effect of probe noise in causality correlations as a function of probe diameter, geometry, Mach number, probe position, etc.

APPENDIX A - PREDICTION OF THE SHAPE OF $\overline{p^{(o)'}p}(\tau)$ INCLUDING THE EFFECT OF SURFACE PROBE NOISE

The relation describing the correlation function $\overline{pp^{(o)'}}(\tau)$ is obtained by multiplying both sides of equation (2.8) by $p^{(o)'}$.

$$(A\text{-}1)\quad p(\underline{x},t)\,p^{(o)'}(o,t'-\tfrac{r}{c}) = \left\{ \frac{1}{4\pi x' c_o}\int_S \cos\theta\left[\frac{\partial p_n}{\partial t}\right]_{t-\frac{x'}{c_o}} ds(\underline{y}') - \frac{1}{4\pi c_o^2 x}\int_V\left[\frac{\partial^2 p^{(o)}}{\partial t^2}\right]_{t-\frac{x}{c_o}} dV(\underline{y})\right\}\cdot p^{(o)'}(o,t'-\tfrac{r}{c_o})$$

$p^{(o)'}$ is the surface pressure measured at 0 (see Figure 5) and is assumed to be $\simeq p^{(o)}$ because of probe design. $p^{(o)'}(0,t'-r/c)$ can be taken inside the integral sign because it is independent of the surface or volume integrals. If the processes are statistically stationary, the left and right hand sides are functions of $\tau=t-t'$ only:

$$(A\text{-}2)\quad \overline{pp^{(o)'}}(\underline{x},\tau+\tfrac{r}{c_o}) = \frac{1}{4\pi x' c_o}\int_S \cos\theta\left[\frac{\partial}{\partial t}\overline{p_n p^{(o)'}}\right]_{\tau+\frac{|r-x'|}{c_o}} ds(\underline{y}') - \frac{1}{4\pi c_o^2 x}\int_V\left[\frac{\partial^2}{\partial t^2}\overline{p^{(o)}p^{(o)'}}\right]_{\tau+\frac{|r-x|}{c_o}} dV(\underline{y})$$

Retarded time differences due to $\underline{r}\neq\underline{x}\neq\underline{x}'$ can be neglected if one assumes that the wavelengths will be generally long compared to the correlation scales, so that A-2 can be simplified to give,

(A-3)

$$\overline{pp^{(o)'}}\left(\underline{x},\tau+\frac{r}{c_o}\right) = \frac{-1}{4\pi x c_o}\int_s \cos\theta\left[\frac{\partial}{\partial\tau}\left(\overline{p_n p^{(o)'}}\right)\right]_\tau ds + \frac{1}{4\pi c_o^2 x}\int_v\left[\frac{\partial^2}{\partial\tau^2}\overline{p^{(o)}p^{(o)'}}\right]_\tau dV$$

I_1 = probe noise effect

I_2 = legitimate jet noise effect

Estimates for I_1 and I_2 must be made in order to evaluate A-3. The procedure for estimating I_1 follows.

Since $\cos\theta=\cos\gamma\cos\beta$ (see Figure 5), then $\int_s p_h \cos\gamma\, ds = F$, the net side force on the probe at an instant due to surface pressure imbalances around the probe. I_1 can now be written as

(A-4) $$I_1 = \frac{-\cos\beta}{4\pi x c_o}\int_{-\infty}^{\gamma_{TIP}}\frac{\partial}{\partial\tau}\left(\overline{p^{(o)}\cdot\frac{\partial F}{\partial y'}}\right)dy'$$

Let $f = \frac{\delta F}{\delta y'}$ = force per unit length. The necessary correlation therefore, is between the measured pressure and the force per unit length along the probe, $\overline{p^{(o)'}f}$. We make two assumptions concerning the form of this correlation:

i) the correlation will decay with distance and time

ii) the correlation will be weighted by the force distribution over the probe surface. In this case, we approximate this distribution by the following function

$$f = K(\gamma_{TIP}-y')\,e^{-(\gamma_{TIP}-y')/kd}$$

The coefficients K and k determine respectively, the magnitude of the force and the distance from the tip at which the function peaks. Both have already been discussed in section 4.

The expression for $\overline{p^{(o)'}f}$ is hence given by:

$$\overline{p^{(o)'}f} = \underbrace{CR}_{\text{These parameters are constants, already discussed in section 4}} \underbrace{K(Y_{TIP}-y')e^{-\frac{(Y_{TIP}-y')}{kd}}}_{\text{form of force distribution}} \underbrace{e^{-\frac{(y'+U_c\hat{\tau})^2}{L^2}}}_{\text{describes the convection and decay with distance; L is a turbulent length scale}} \underbrace{e^{-\frac{\hat{\tau}^2}{T^2}}}_{\text{describes decay with time; T is a typical decay time of turbulence}}$$

Substituting the expression for $\overline{p^{(o)'}f}$ into I_1, we get:

$$\text{(A-5)}\quad I_1 = -\frac{\cos\beta\, RK}{4\pi x c_o}\int_o^\infty \frac{\partial}{\partial\tau}\, z\, e^{-z/kd-\frac{(Y_t-y'+U_c\hat{\tau})^2}{L^2}-\frac{\hat{\tau}^2}{T^2}}\, dz$$

where $z=Y_t-y'$. Differentiating with respect to τ, I_1 becomes:

$$\text{(A-6)}\quad I_1 = \frac{\cos\beta\, RK}{4\pi x c_o}\, e^{-\frac{\hat{\tau}^2}{T^2}}\int_o^\infty z\, e^{-z/kd-\frac{(Y_T-z+U_c\hat{\tau})^2}{L^2}} \times \left(g - 2z\frac{U_c}{L^2}\right) dz$$

where $g = \frac{2\hat{\tau}}{T^2} + \frac{2U_c^2\hat{\tau}}{L^2} + \frac{2Y_tU_c}{L^2}$. The exponent of the exponential in A-6 can be put into the form $-az^2-2bz-c$ where $a = \frac{1}{L^2}$; $b = \frac{1}{2kd} - \frac{U_c\hat{\tau}}{L^2} - \frac{Y_t}{L^2}$; and $c = \frac{Y_t^2 + (U_c\hat{\tau})^2 + 2Y_tU_c\hat{\tau}}{L^2}$. I_1 can now be written as two standard

integrals:

$$(A\text{-}7)\quad I_1 = \cos\beta\, Rk\, e^{-\hat{\tau}^2/T^2}\left\{ g\int_0^\infty z\, e^{-az^2-2bz-c}\, dz - \frac{2U_c}{L^2}\int_0^\infty z^2 e^{-az^2-2bz-c}\, dz \right\}$$

$$(A\text{-}8)\quad I_1 = \cos\beta\, Rk\, e^{-\hat{\tau}^2/T^2}\left\{ g\left(\frac{1}{2a}\sqrt{\frac{\pi}{a}}\, e^{\frac{b^2}{a}-c}\, \mathrm{erfc}\,\frac{b}{\sqrt{a}}\right) - \frac{2U_c}{L^2}\left(-\frac{b}{2a^2}e^{-c} + \left(\sqrt{\frac{\pi}{a^5}}\,\frac{(2b^2+a)}{4}\, e^{\frac{b^2}{a}-c}\, \mathrm{erfc}\,\frac{b}{\sqrt{a}}\right)\right)\right\}$$

Substituting the expressions for a, b and c, but defining a new variable $Q = \frac{L^2}{kd} - U_c\hat{\tau} - Y_t$, the following can be written:

$$(A\text{-}9)\quad I_1 = \cos\beta\, Rk\, e^{-\hat{\tau}^2/T^2}\, e^{2/kd\,(\frac{L^2}{2kd} - U_c\hat{\tau} - Y_t)}\, \mathrm{erfc}\,(Q/L)\left\{\left(\frac{\hat{\tau}L^2}{U_cT^2} + U_c\hat{\tau} + Y_t\right)U_cL\sqrt{\pi} + \frac{U_cQe^{-Q^2/L^2}}{\mathrm{erfc}\,(Q/L)} - U_c\sqrt{\pi}\,(Q^2/L + L/2)\right\}$$

To estimate I_2, it has been common to assume a convecting Gaussian for the jet pressure correlation:

$$\overline{p^{(o)'}p^{(o)}}(\tau) = \overline{p^{(o)2}}\, e^{-\frac{(Y_1 - U_c\hat{\tau})^2}{L_1^2} - \frac{Y_2^2}{L_2^2} - \frac{Y_3^2}{L_3^2} - \frac{\hat{\tau}^2}{T^2}}$$

I_2 becomes then,

$$I_2 = -\frac{1}{4\pi C_0^2 x}\frac{\partial^2}{\partial\tau^2}\int_{y_1}\int_{y_2}\int_{y_3}\overline{p^{(o)^2}}\, e^{-\frac{(y_1-u_c\hat{\tau})}{L_1^2}-\frac{y_2^2}{L_2^2}-\frac{y_3^2}{L_3^2}-\frac{\hat{\tau}^2}{T^2}}dy_1\,dy_2\,dy_3$$

(A-10)

The limits will be at infinity for each integration.

(A-11)

$$I_2 = -\frac{\overline{p^{(o)^2}}}{4\pi C_0^2 x}\left(\frac{1}{2}\sqrt{\frac{\pi}{1/L_3^2}}\ \mathrm{erf}\left(\sqrt{1/L_3^2}\cdot x\right)\right|_{-\infty}^{\infty}$$

$$\frac{\partial^2}{\partial\tau^2}\int_{y_1}\int_{y_2} e^{-\frac{(y_1-u_c\tau)^2}{L_1^2}-\frac{y_2^2}{L_2^2}-\frac{\tau^2}{T^2}}\,dy_1\,dy_2$$

$$= -\frac{\overline{p^{(o)^2}}\sqrt{\pi}\,L_3}{4\pi C_0^2 x}\frac{\partial^2}{\partial\tau^2}\int_{y_1}\int_{y_2} e^{-\frac{(y_1-u_c\hat{\tau})^2}{L_1^2}-\frac{y_2^2}{L_2^2}-\frac{\hat{\tau}^2}{T^2}}\,dy_1\,dy_2$$

Similarly, the integration in the directions y_1 and y_2 will lead to

(A-12)

$$I_2 = -\frac{\overline{p^{(o)^2}}\,L_1L_2L_3\sqrt{\pi}}{4C_0^2 x}\frac{\partial^2}{\partial\tau^2}\left(e^{-\hat{\tau}^2/T^2}\right)$$

$$= \frac{\overline{p^{(o)^2}}\,L_1L_2L_3\sqrt{\pi}}{2C_0^2 x T^2}\left\{e^{-\hat{\tau}^2/T^2}\left(1-\frac{2\hat{\tau}^2}{T^2}\right)\right\}$$

The correlation $\overline{p^{(o)'}p(\tau)}$ is the sum of I_1 and I_2 (as given in A-3):

$$\overline{p^{(o)}P(\tau)} = \frac{\cos\beta\, Rk}{4\pi x C_0}e^{-\hat{\tau}^2/T^2}\,e^{2/kd\left(L^2/2kd-u_c\hat{\tau}-Y_T\right)}\,\mathrm{erfc}\,(Q/L)$$

$$\left\{\left(\frac{\hat{\tau}L_1^2}{u_cT^2}+u_c\hat{\tau}+Y_T\right)u_cL\sqrt{\pi}+u_cQe^{-Q^2/L_1^2}-u_c\sqrt{\pi}\left(\frac{Q^2}{L}+\frac{L}{2}\right)\right\}$$

$$+\ \frac{\overline{p^{(o)^2}}\,L_1L_2L_3\sqrt{\pi}}{2C_0^2 x T^2}\left\{e^{-\hat{\tau}^2/T^2}\left(1-2\frac{\hat{\tau}^2}{T^2}\right)\right\}$$

APPENDIX B - STATIC PRESSURE MEASUREMENT IN A TURBULENT FLOW[15]

If a standard probe is measuring static pressure in a turbulent field, then the pressure error caused by unsteady cross-components of velocity can be approximated by the pressure distribution on a long cylinder in ideal cross-flow. The pressure at the surface of the probe, subtracted by the pressure which would have occurred in the absence of the probe will be given by:

$$P_m(\theta,t) - P_{TRUE}(t) = \tfrac{1}{2}\rho V_n^2 (1-4\sin^2\theta) + \rho \dot{V}_n d\cos\theta$$

where V_n is the component of velocity normal to the cylinder.

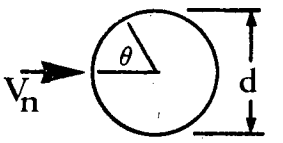

If the pressure probe averages the circumferential pressure perfectly, then for ideal flow the second term will be zero and the first term will be $-\frac{1}{2}\rho V_n^2(t)$. A real probe with a finite number of pressure taps, will not take an exact average over the circumference of the cylinder, so that the term due to acceleration will contribute to the error. If more than three taps are used, the inaccuracy in averaging over the circumference will be small, so that the error due to the acceleration term will be much less than the error due to the velocity term. For real flows, the error due to the velocity term can be given by $P_m(t) - P_t(t) = B\rho V_n^2(t)$ where B must be evaluated from quasi-steady flow calibrations ($B = -\frac{1}{2}$ for potential flow). Siddon found values of B between -.31 and -.46, and Planchon reports -.5 .

If the pressure and velocity terms are written in terms of mean and fluctuating quantities, then the unsteady pressure error can be written as:

$$P_m(t) - P_t(t) = B\rho\,(v_n^2 - \overline{v_n^2})$$

where $v_n^2 = v^2 + w^2$. Squaring and time averaging,

$$\overline{(P_m - P_t)^2} = (B\rho)^2\left(\overline{(v_n^2)^2} + \overline{(v_n^2)}^2 - 2\,\overline{v_n^2}\;\overline{v_n^2}\right)$$

The ratio $\overline{v_n^4}/(\overline{v_n^2})^2 \simeq 2$ for a jet shear layer, therefore

$$\overline{(P_m - P_t)^2} = (B\rho)^2\,\overline{(v_n^2)}^2$$

If the true jet pressure $\simeq .05\rho V_j^2$, then the fractional error in the rms pressure can be written as:

$$\frac{\overline{(P_m - P_t)}}{.05\,\rho V_j^2} = \frac{B\rho\,(\overline{v_n^2})}{.05\,\rho V_j^2}$$

Considering the worst case, $B = -\frac{1}{2}$, $v_n^2 = .15U_j$, the fractional error will be

$$\frac{\overline{(P_m - P_t)}}{.05\,\rho V_j^2} = -\frac{.5\,(.15)^2}{.05} = .225$$ i.e., the expected error will not exceed 22.5%.

REFERENCES

1. Chu,W.T., "Turbulence Measurements Relevant to Jet Noise",UTIAS Report No. 119, November (1966).

2. Curle, N., "The Influence of Solid Boundaries Upon Aerodynamic Sound", Proc Roy. Soc. A, 231, 505-514, (1955).

3. Dean, R.C., "Aerodynamic Measurements", MIT Press, Cambridge, Mass., (1953).

4. Fuchs, H.V., Michalke, A., "Four Introductory Lectures on Aerodynamic Noise Theory", Deutsche Luft-und Raumfahrt Mitteilung 71-20, (1971).

5. Lee, H.K., "Correlation of Noise and Flow of a Jet", UTIAS Rep. 168 (1971)

6. Lee, H.K., Ribner, H.S., "Direct Correlation of Noise and Flow of a Jet", J.Acoust.Soc.Am., Vol. 52. Number 5 part 1,p1280,(1972).

7. Liepmann, H.W., Roshko, A., "Elements of Gasdynamics", John Wiley & Sons, New York, (1957).

8. Meechan, W.C., Hurdle, P.M., and Hodder, B., "Investigations of the Aerodynamic Noise Generating Region of a Jet Engine by Means of the Simple Source Fluid Dilatation Model", JASA, Vol. 56, No. 6 (1974).

9. Nayer,B.M.,Siddon, T.E., and Chu, W.T., "Properties of the Turbulence in the Transition Region of a Round Jet", Univ. of Toronto Inst. for Aerospace Studies T.N.-131 (1974)

10. Planchon, H.P.,"The Fluctuating Static Pressure Field in a Round Jet Turbulent Mixing Region", PhD Thesis, Nuclear Engineering Program,

11. Proudman, I., "The Generation of Noise by Isotropic Turbulence", Proc. Roy.Soc. A, Vol.214, p.119. (1952).

12. Rackl, R., "Two Causality Correlation Techniques Applied to Jet Noise", PhD Thesis, Dept. of Mech. Eng., University of British Columbia, April (1973).

13. Ribner, H.S., "The Generation of Sound by Turbulent Jets", Advances in Applied Mechanics. Vol. 8, Academic Press Inc., New York, 1964.

14. Scharton, T.D., White, P.H., "Simple Pressure Source Model of Jet Noise" J.Acoust.Soc.Am., Vol.52, Part 1, July (1972).

15. Siddon, T.E., "On the Response of Pressure Measuring Instrumentation in Unsteady Flow", UTIAS Rep. No. 136, January (1969)

16. Siddon, T.E., "Surface Dipole Strength by Cross-Correlation Method", J.Acoust.Soc.Am., Vol.53, No.2, p.619-633, Feb. (1973).

17. Siddon, T.E., "Noise Source Diagnostics Using Causality Correlations", Specialists Meeting on Noise Mechanisms, AGARD Fluid Dynamics Panel, Belgium, Sept. (1973).

18. Siddon, T.E., "Some Observations on Source Detection Methods With Application to Jet Noise", published in Proceedings of the 2nd Interagency Symposium on University Research in Transportation Noise, North Carolina University.

19. Smith, R.H., Wang, C.Y., "Contracting Cones Giving Uniform Throat Speeds". Jour. Aeor. Sci., Vol.11, p.356-360, (1944).

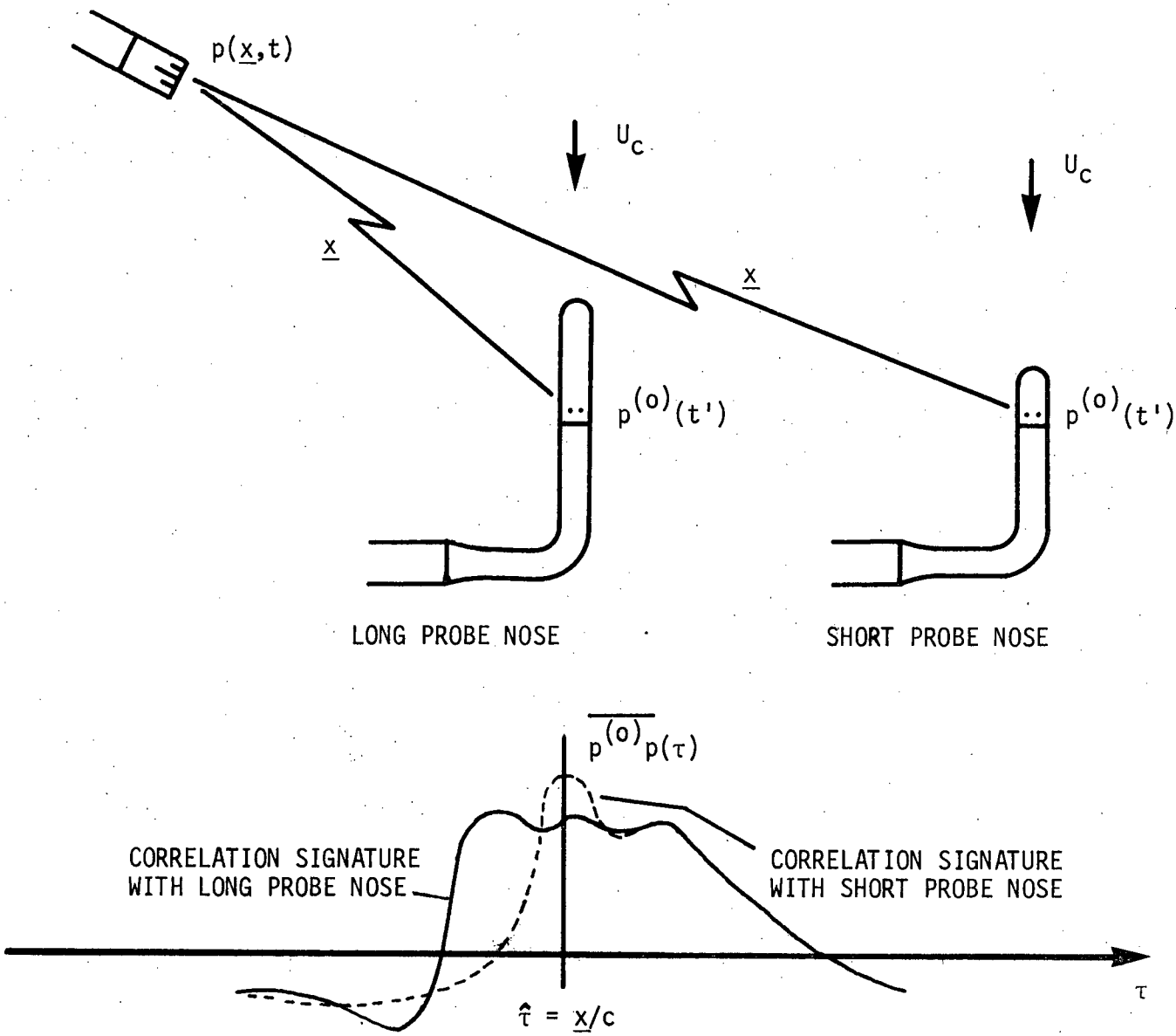

Figure 1 - The Effect of Probe Nose Length on the Cross-Correlation Signature

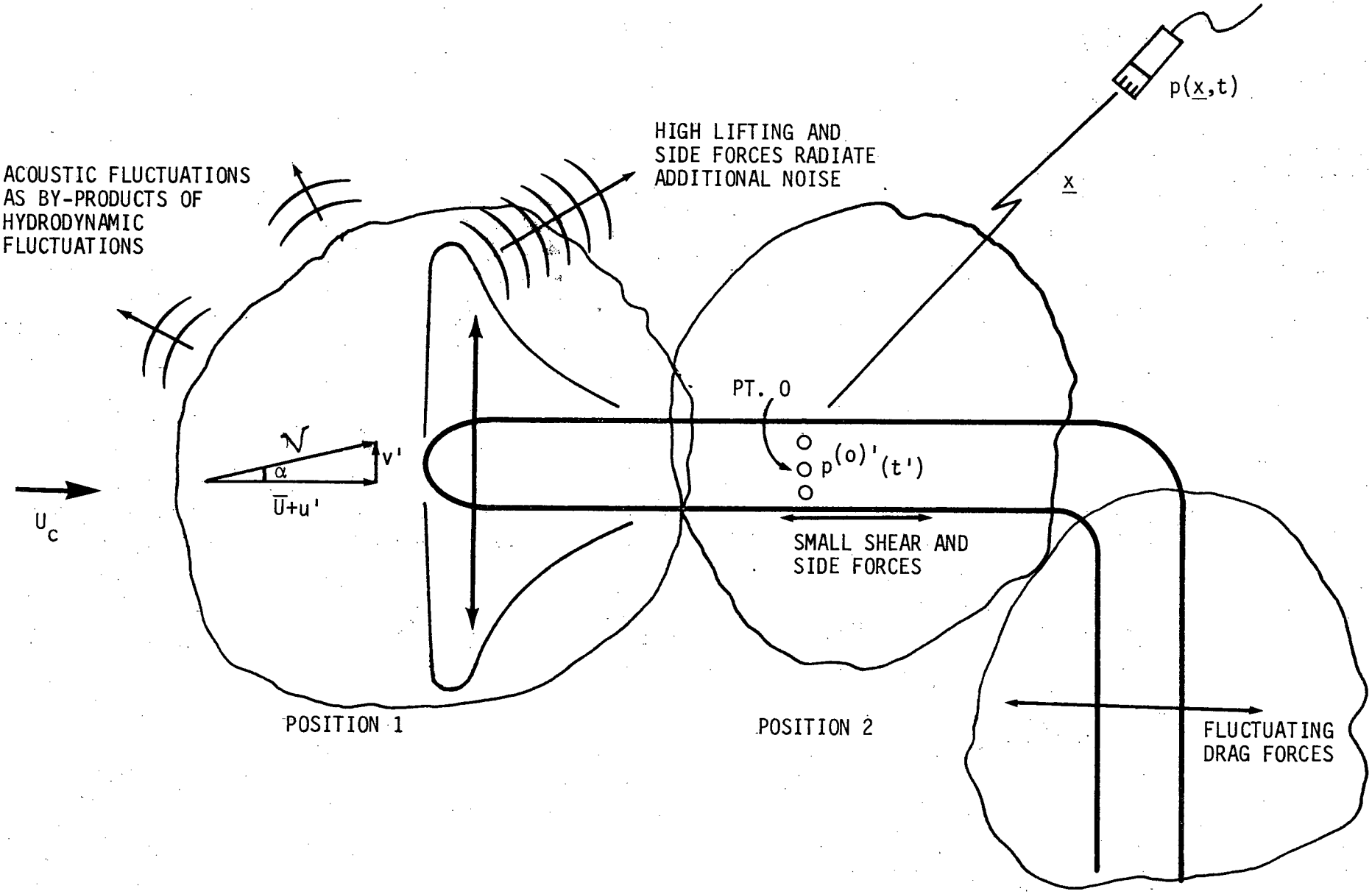

Figure 2 - A Probe Imbedded in a Turbulent Flow

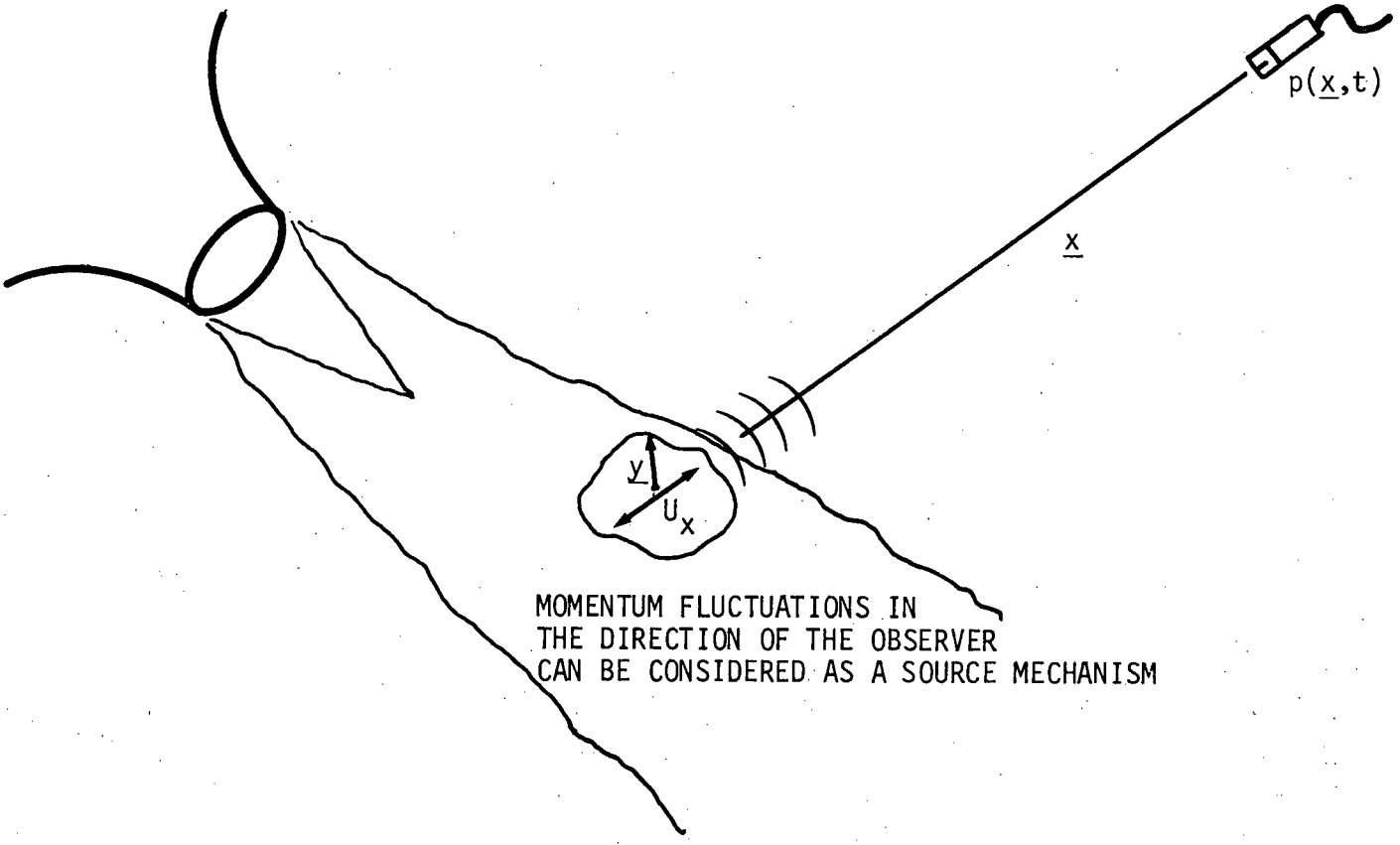

Figure 3 - The Proudman Source Mechanism

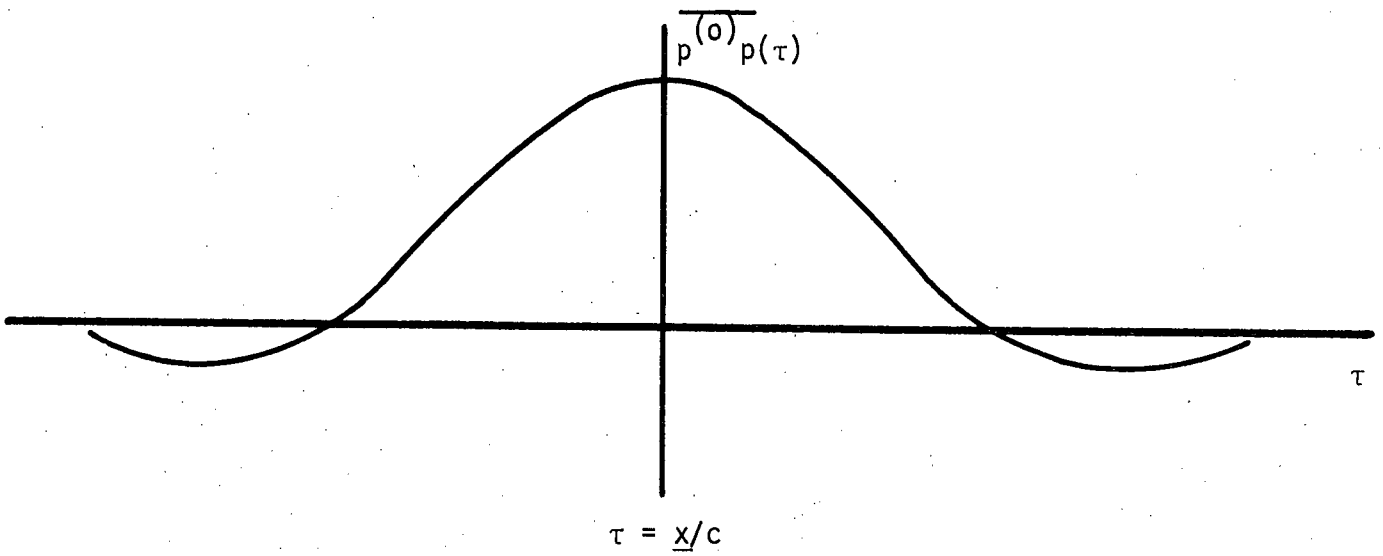

Figure 4 - A Hypothetical Causality Correlation Function for Pure Jet Noise

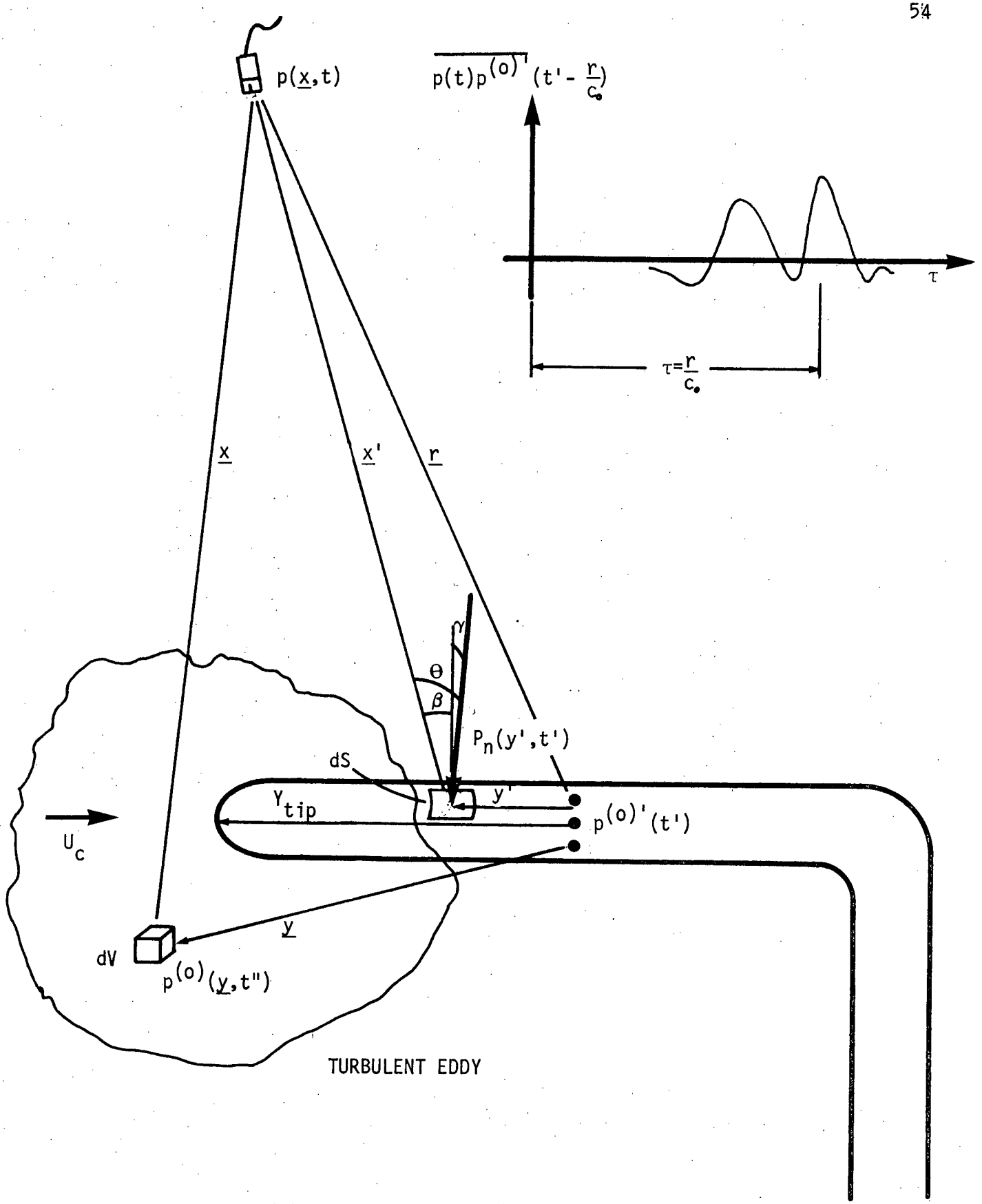

Figure 5 - Geometry Used For the Prediction of $\overline{pp^{(o)'}}(\tau)$

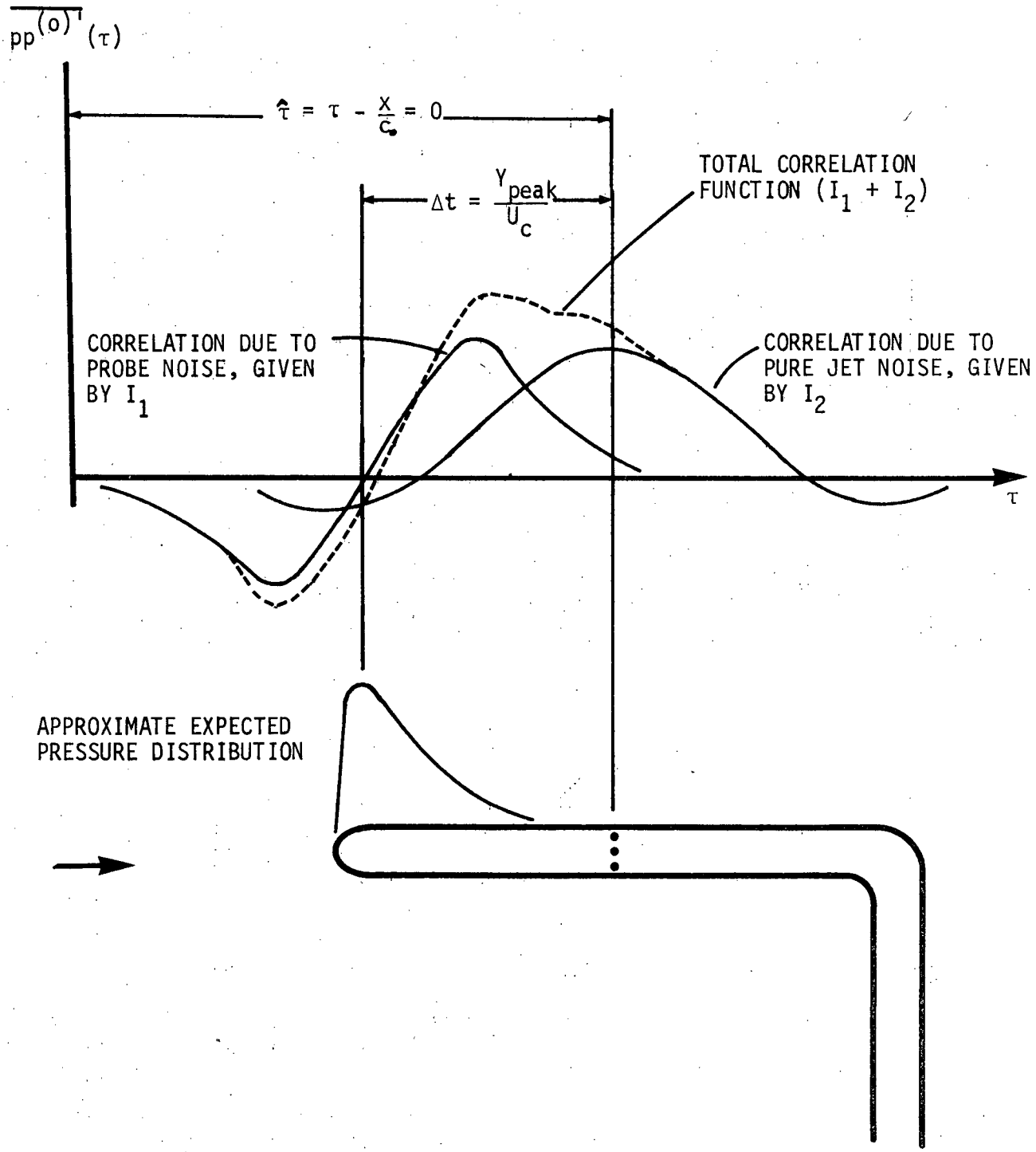

Figure 6 - Hypothetical Correlation Function For a Standard Probe

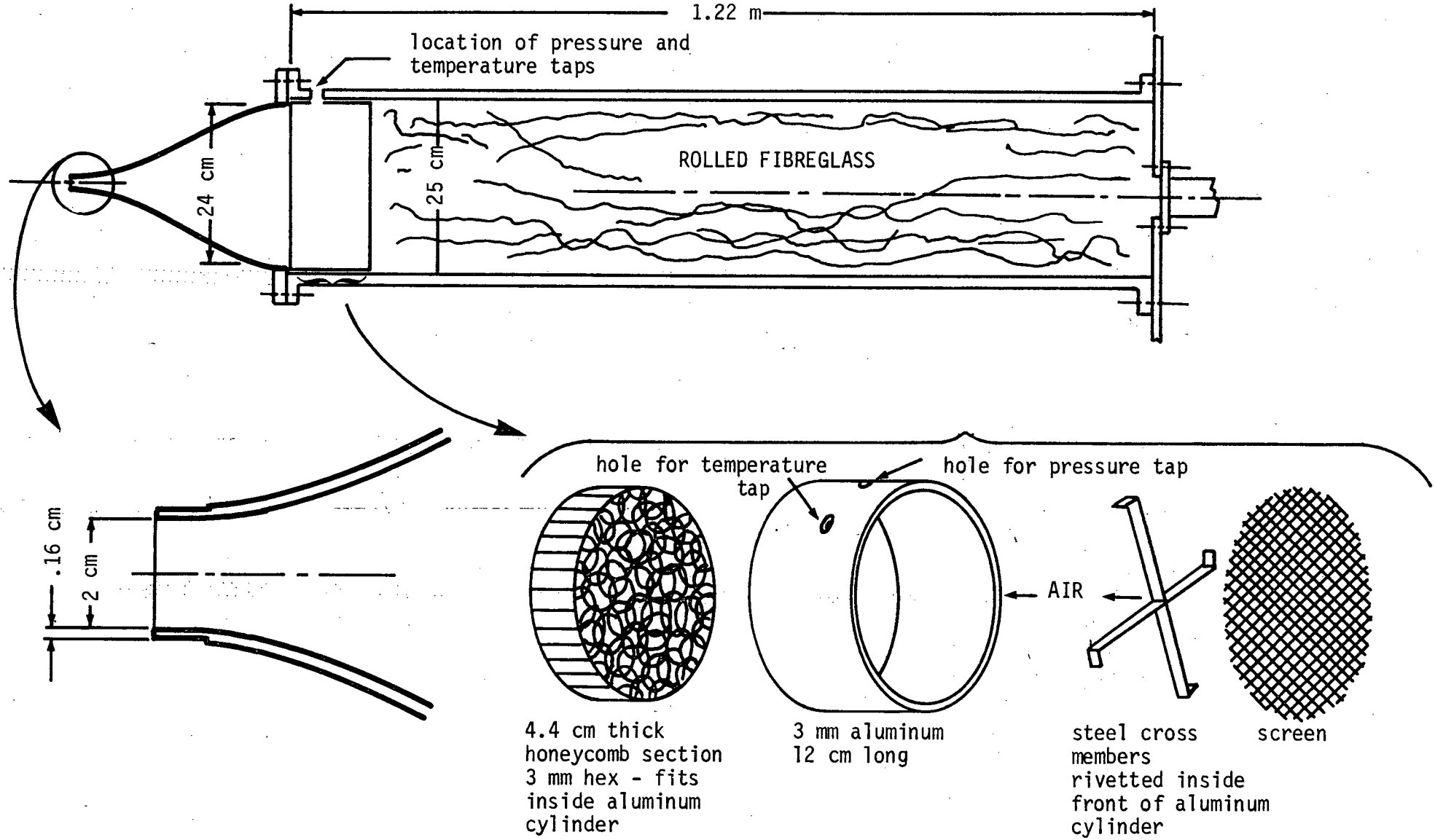

Figure 7 - Jet Plenum and Nozzle

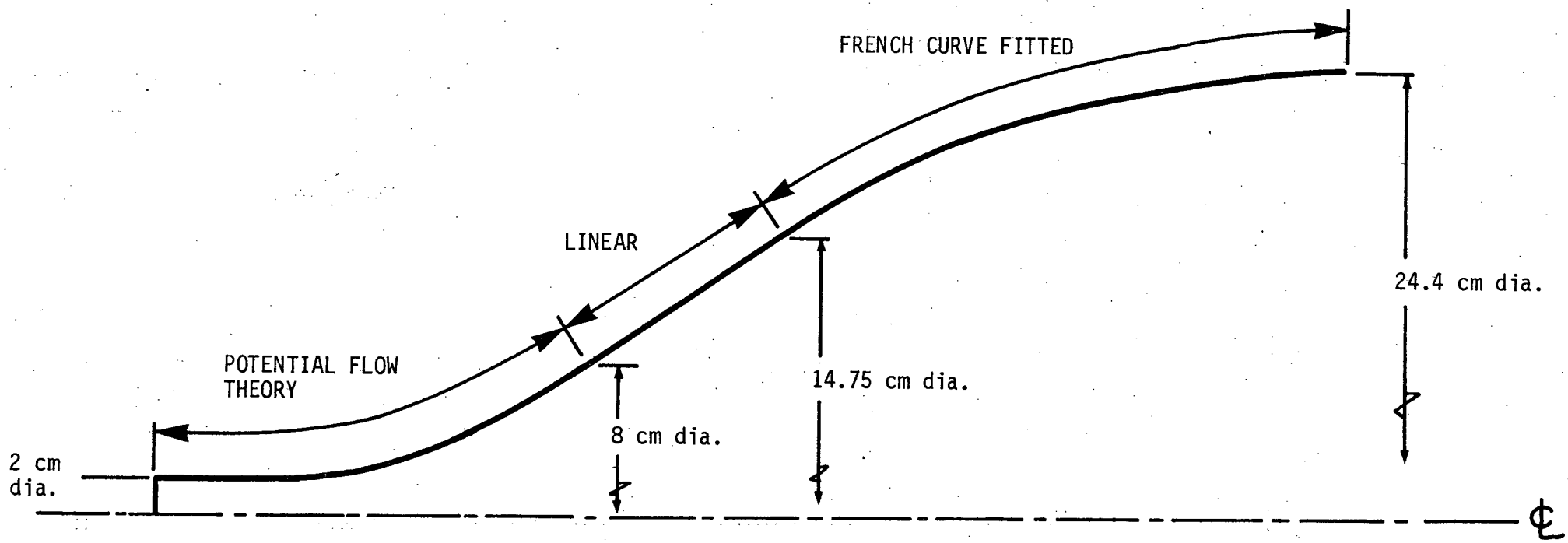

Figure 8 - Schematic of Contoured Nozzle

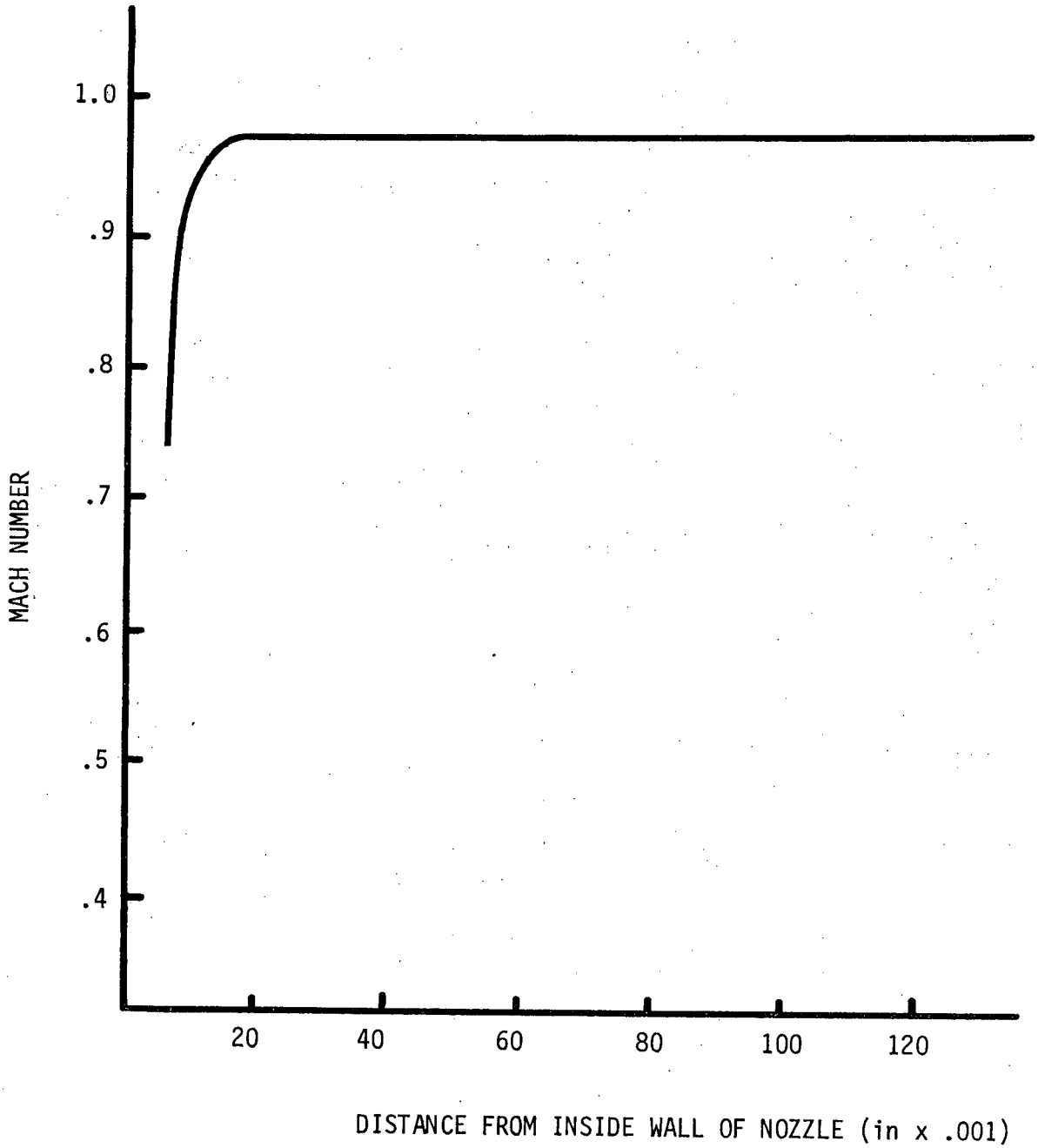

Figure 9 - Mean Velocity Profile at the Jet Exit Plane at M = .99

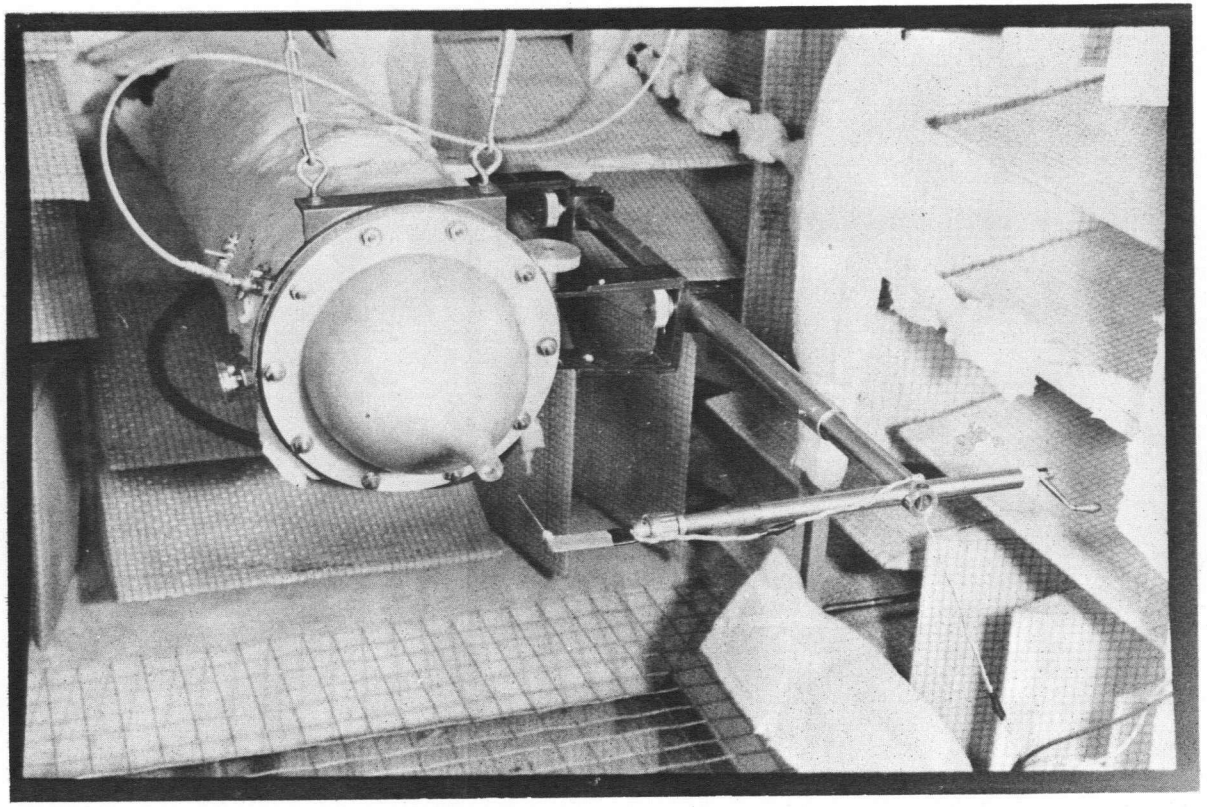

Figure 10 - Experimental Set-up Showing Traversing Mechanism

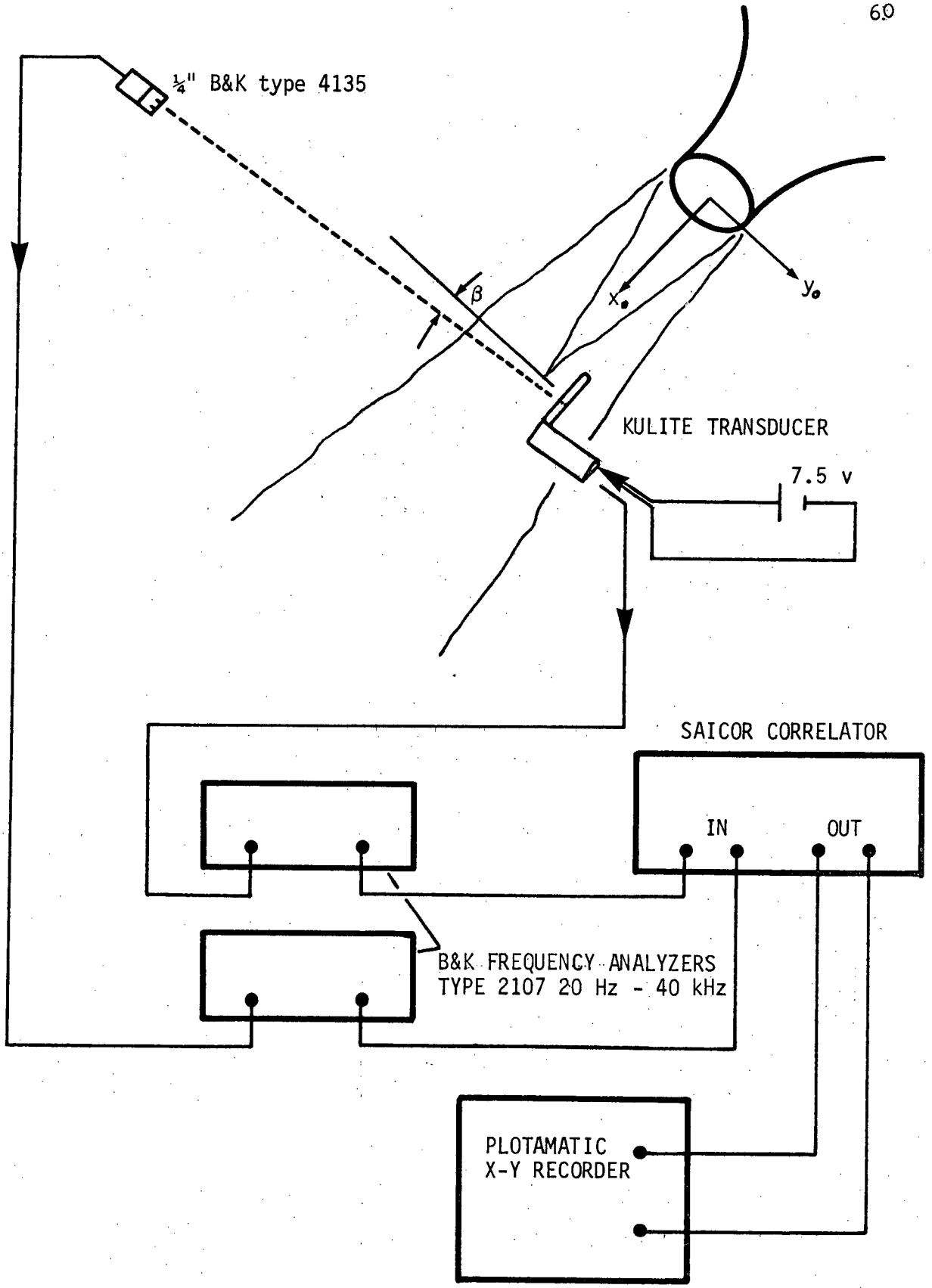

Figure 11 - Signal Paths

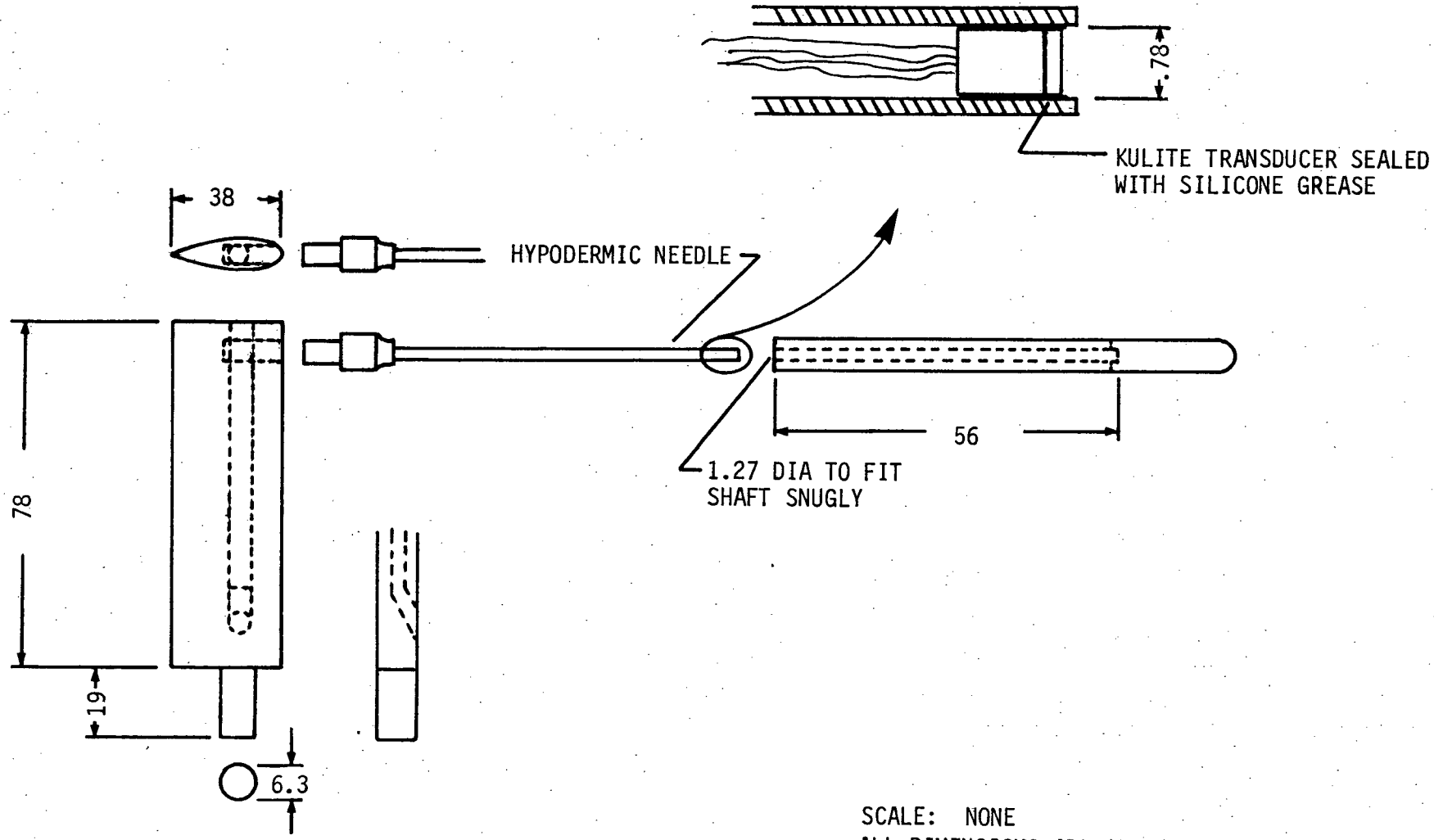

Figure 12 - Construction Details of Kulite Probe Holder

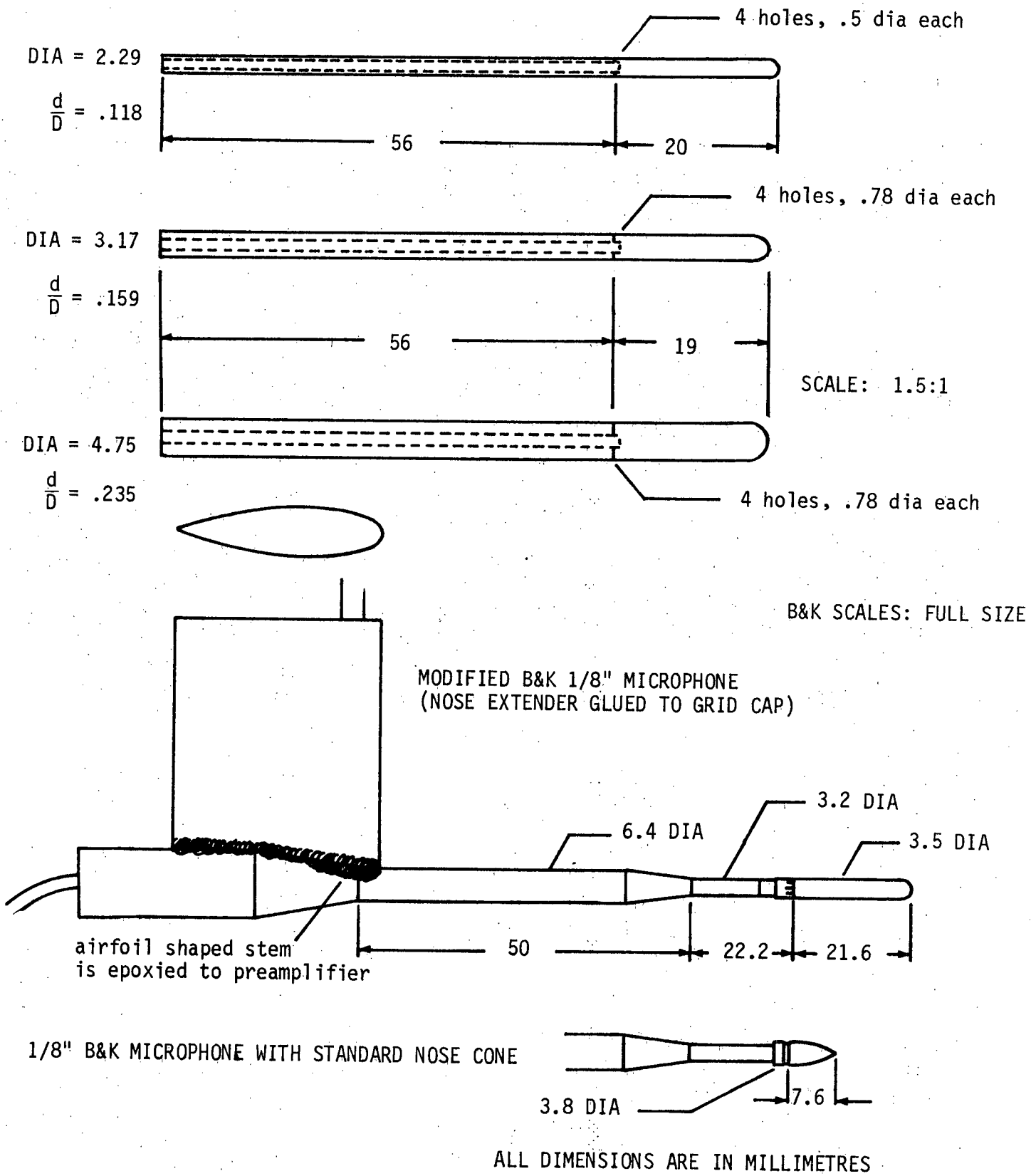

Figure 13 - Details of All In-Flow Probes

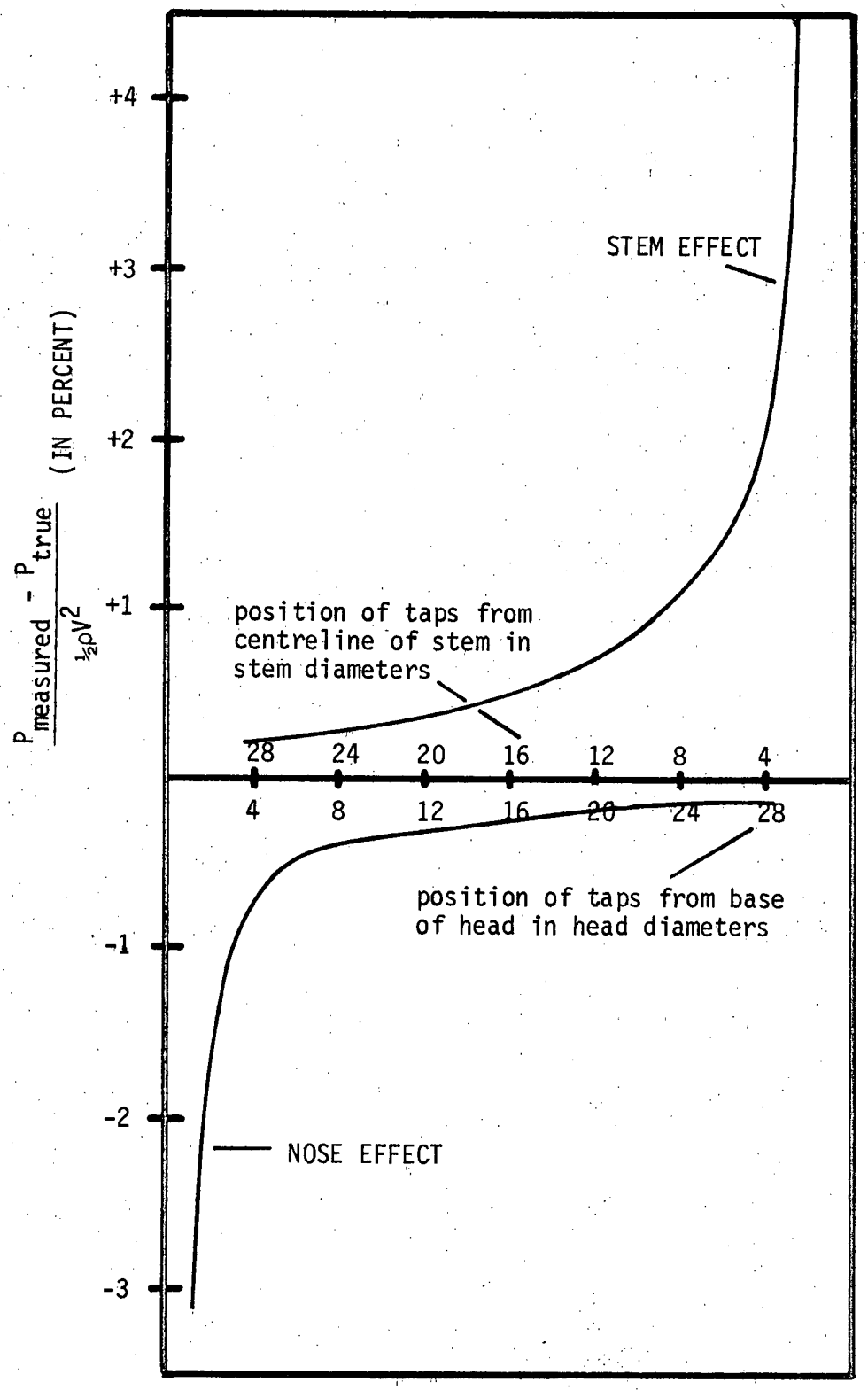

Figure 14[3] - Probe Tip and Stem Effects For a Standard Probe in Steady Flow

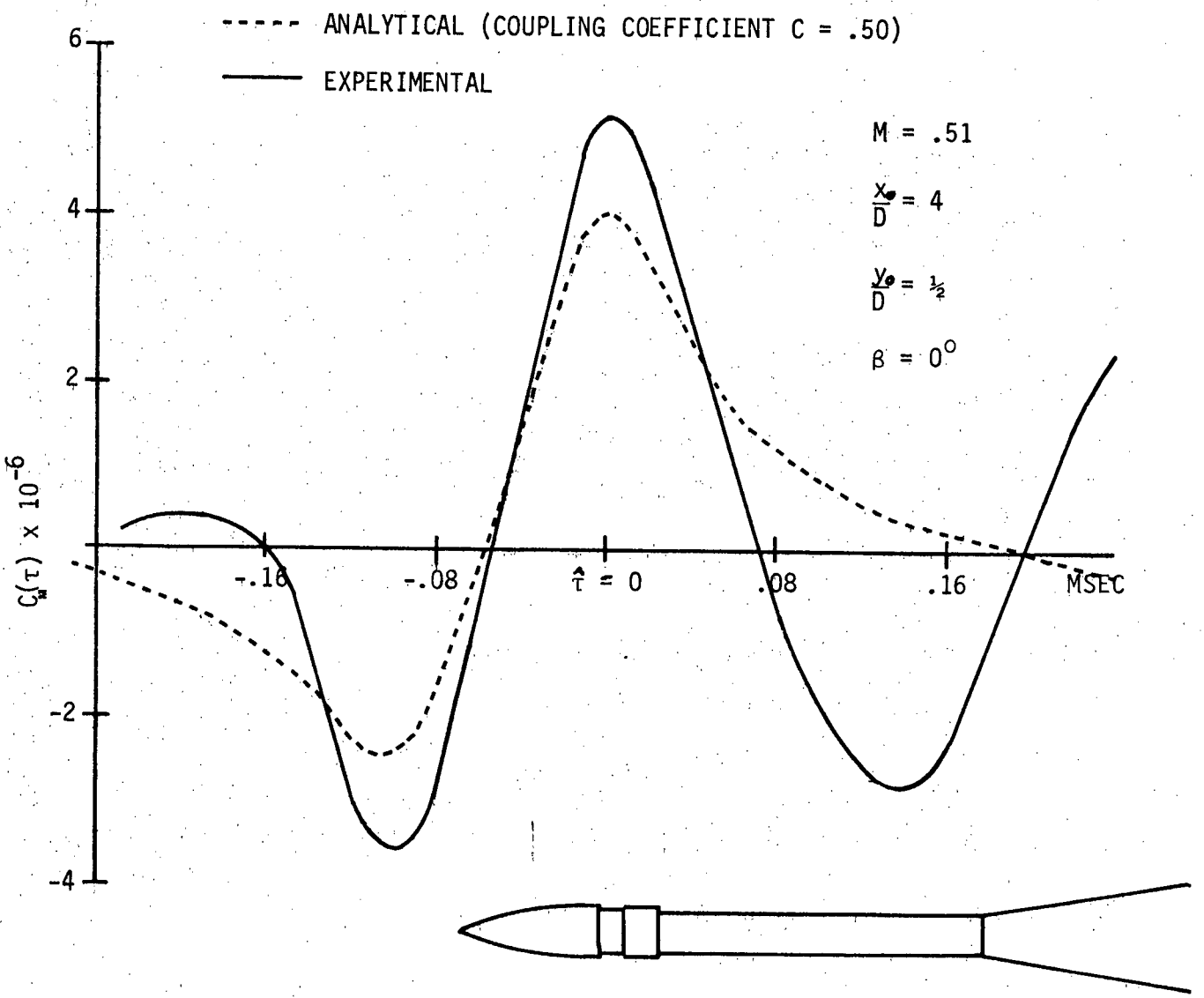

Figure 15 - Experimental and Analytical Causality Correlations Using a Standard 1/8" B&K Microphone With a Nose Cone

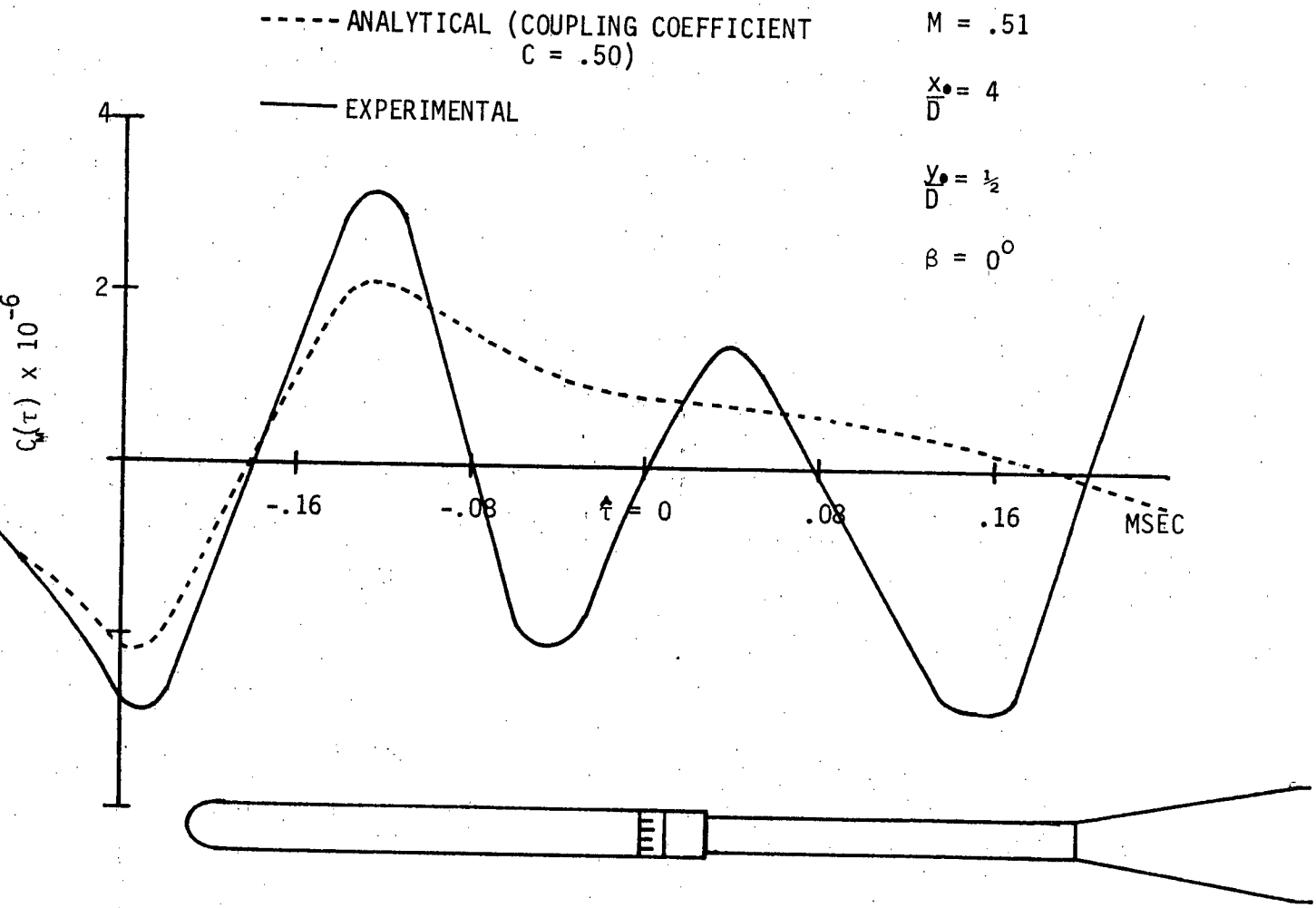

Figure 16 - Experimental and Analytical Causality Correlation For a Modified 1/8" B&K Microphone

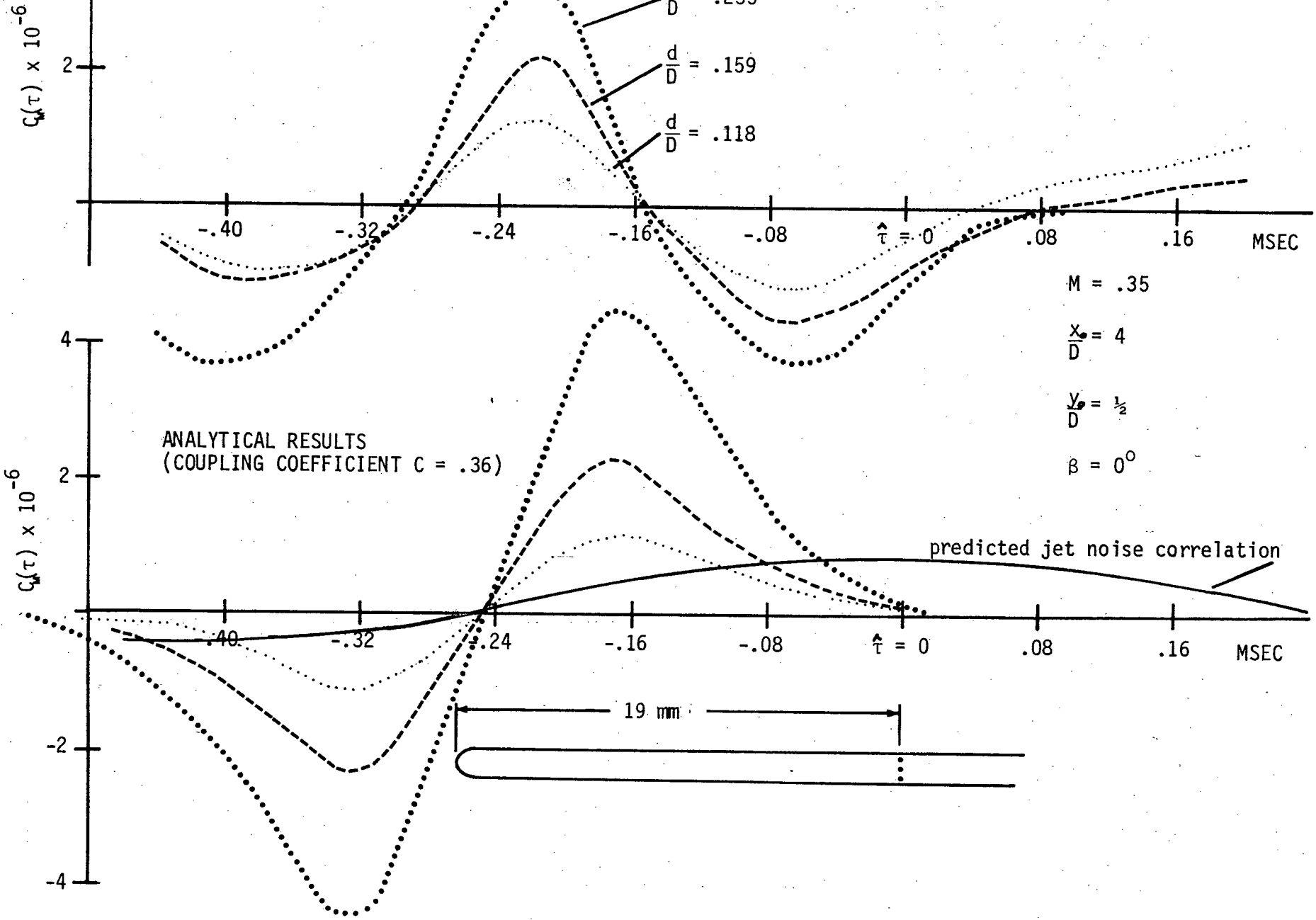

Figure 17 - Experimental and Analytical Causality Correlations
M = .35

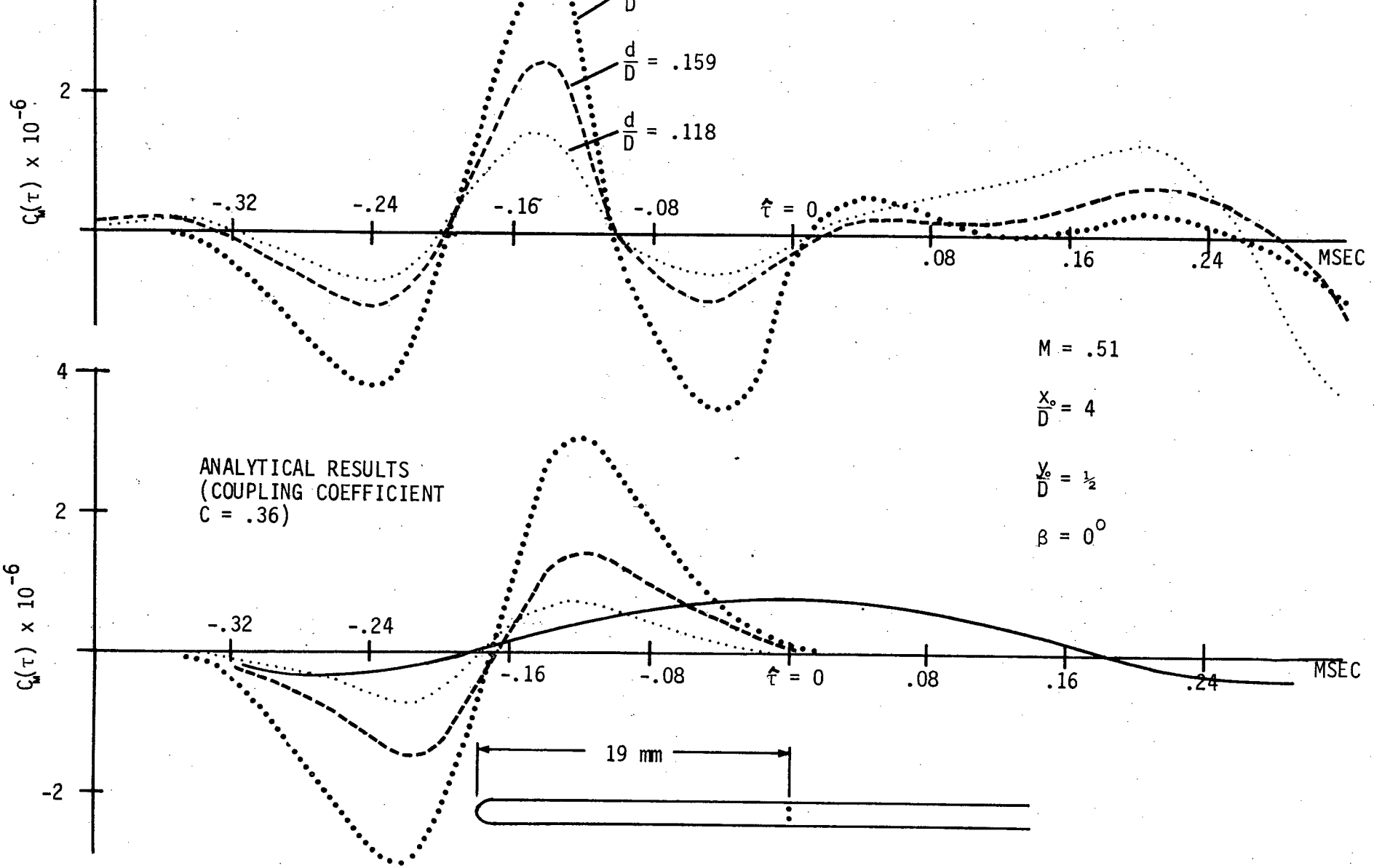

Figure 18 - Experimental and Analytical Causality Correlations
M = .51

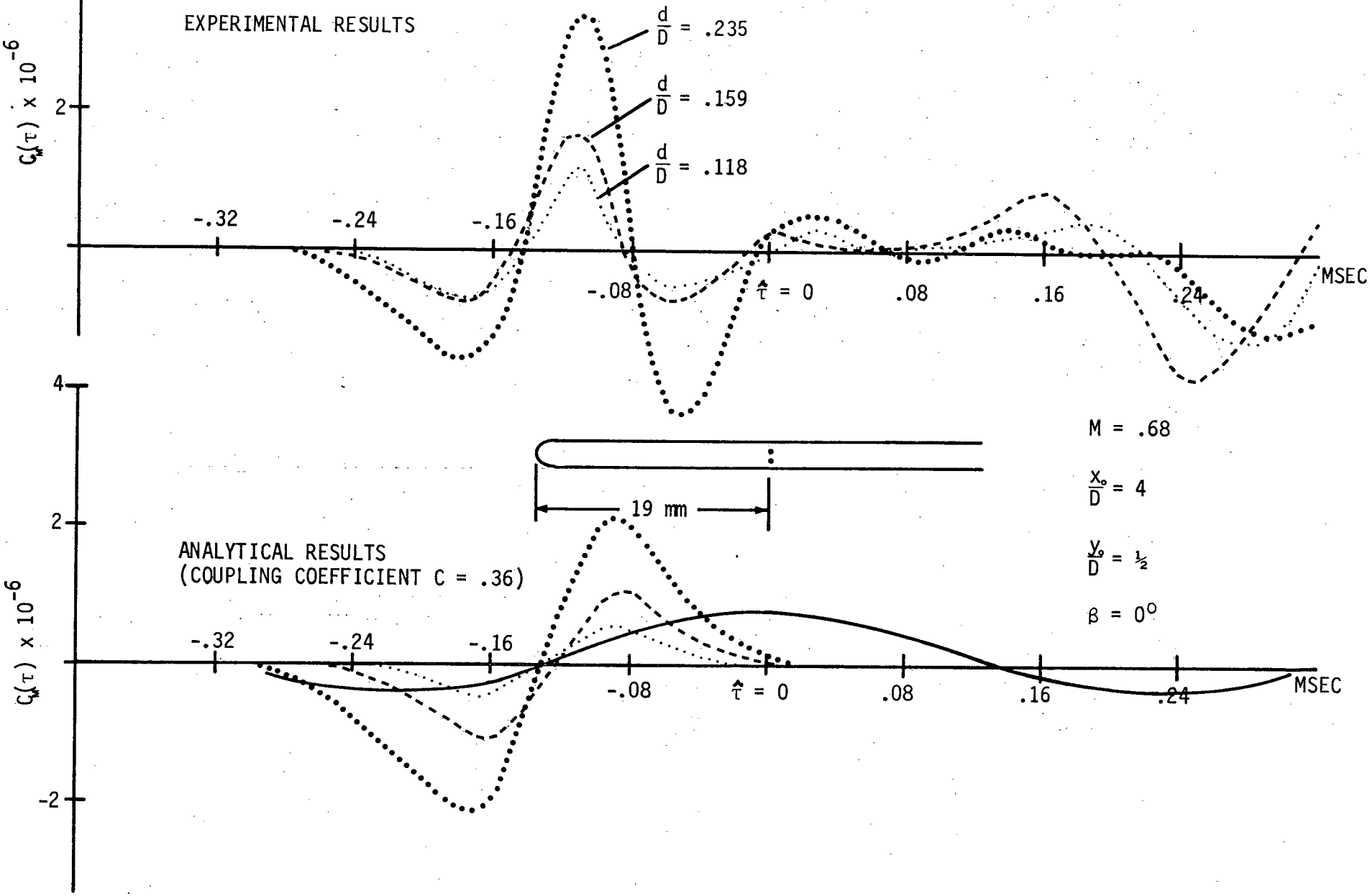

Figure 19 - Experimental and Analytical Causality Correlations
M = .68

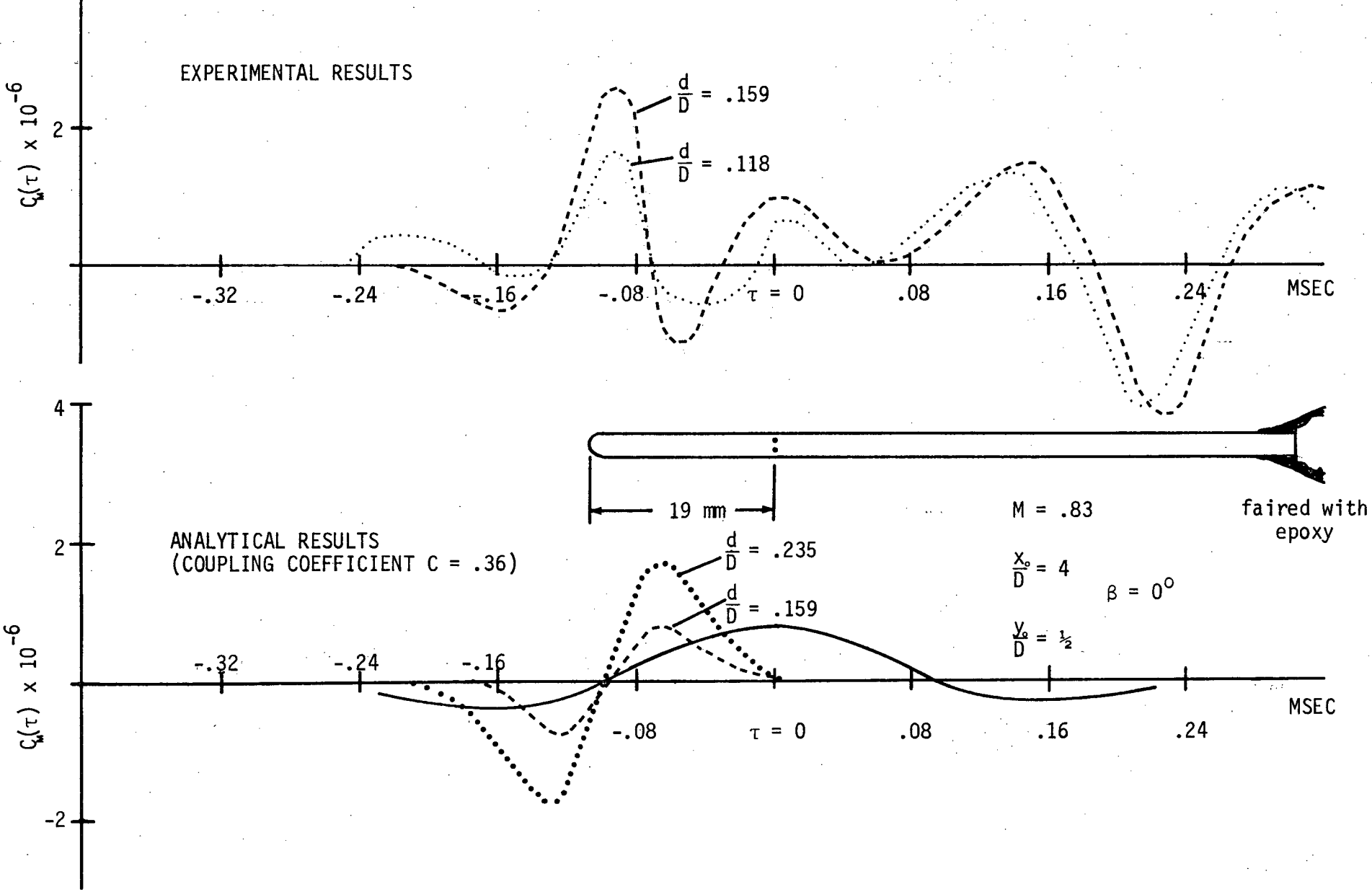

Figure 20 - Experimental and Analytical Causality Correlations
M = .83

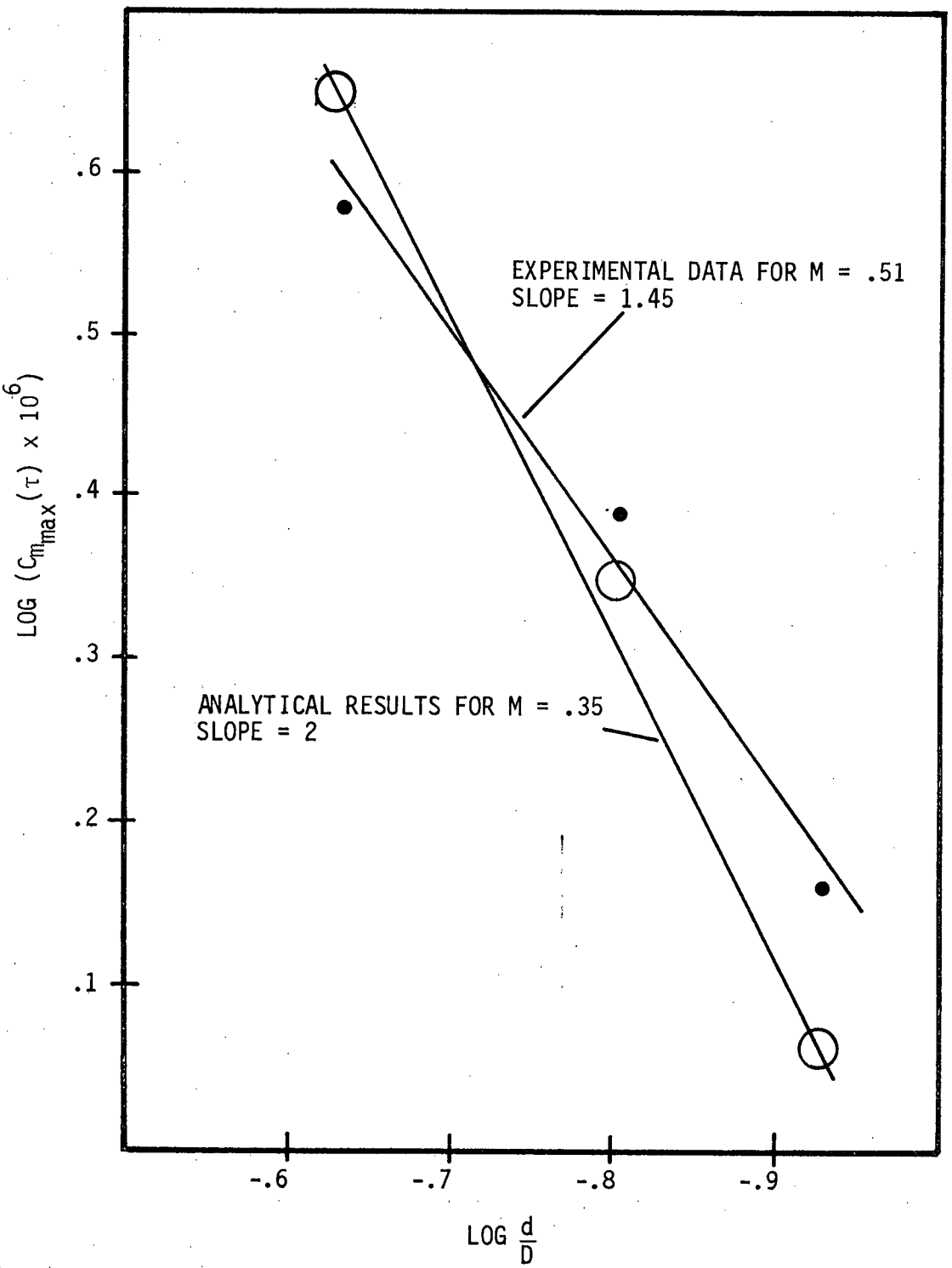

Figure 21 - Log $C_{m_{max}}(\tau)$ Versus Log $\frac{d}{D}$

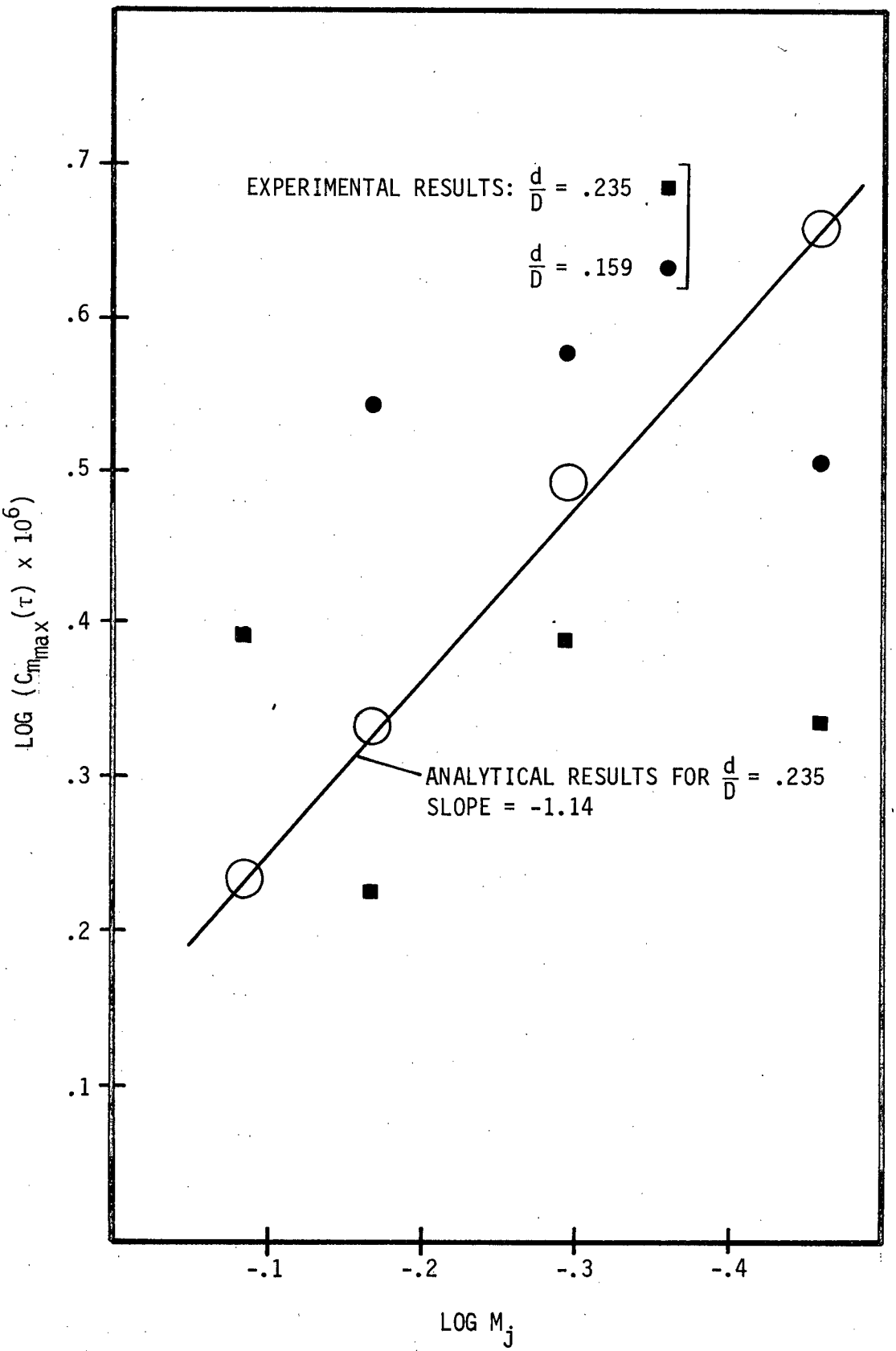

Figure 22 - Log $C_{m_{max}}(\tau)$ Versus Log M_j

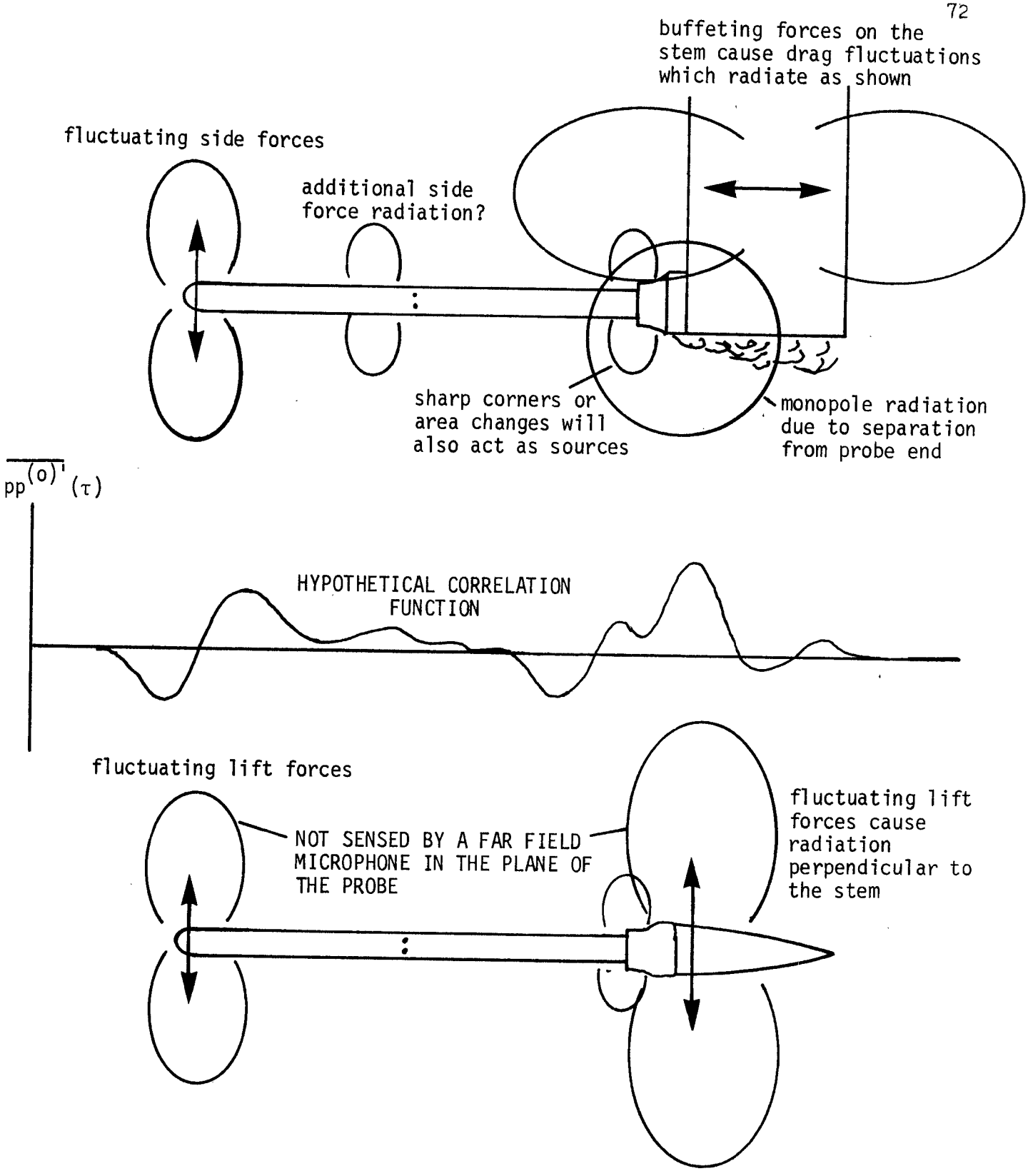

Figure 23 - Possible Sources of Probe Noise on the Kulite Probes Used